Environmental Science and Pollution Research (2019) 26:2203–2227
https://doi.org/10.1007/s11356-018-3595-5

REVIEW ARTICLE

As(III) and Cr(VI) oxyanion removal from water by advanced oxidation/reduction processes—a review

Belisa A. Marinho[1,2] · Raquel O. Cristóvão[1] · Rui A. R. Boaventura[1] · Vítor J. P. Vilar[1]

Received: 12 April 2018 / Accepted: 24 October 2018 / Published online: 24 November 2018

Abstract

Water pollution by human activities is a global environmental problem that requires innovative solutions. Arsenic and chromium oxyanions are toxic compounds, introduced in the environment by both natural and anthropogenic activities. In this review, the speciation diagrams of arsenic and chromium oxyanions in aqueous solutions and the analytical methods used for their detection and quantification are presented. Current and potential treatment methods for As and Cr removal, such as adsorption, coagulation/flocculation, electrochemical, ion exchange, membrane separation, phyto- and bioremediation, biosorption, biofiltration, and oxidative/reductive processes, are presented with discussion of their advantages, drawbacks, and the main recent achievements. In the last years, advanced oxidation processes (AOPs) have been acquiring high relevance for the treatment of water contaminated with organic compounds. However, these processes are also able to deal with inorganic contaminants, mainly by changing metal/metalloid oxidation state, turning these compounds less toxic or soluble. An overview of advanced oxidation/reduction processes (AO/RPs) used for As and Cr removal was carried out, focusing mainly on H_2O_2/UVC, iron-based and heterogeneous photocatalytic processes. Some aspects related to AO/RP experimental conditions, comparison criteria, redox mechanisms, catalyst immobilization, and process intensification through implementation of innovative reactors designs are also discussed. Nevertheless, further research is needed to assess the effectiveness of those processes in order to improve some existing limitations. On the other hand, the validation of those treatment methods needs to be deepened, namely with the use of real wastewaters for their future full-scale application.

Keywords Inorganic pollutants treatment · Iron-based processes · UVC/H_2O_2 · Heterogeneous photocatalysis · Photocatalyst immobilization · Process intensification

Highlights
- Description of Cr(VI) and As(III) speciation diagrams and the analytical methods for their detection
- Report on common treatment methods for arsenic and chromium removal
- Review on recent advances of Cr(VI) and As(III) treatment by AO/RPs
- Last advances in intensification of heterogeneous photocatalytic processes

Responsible editor: Philippe Garrigues

✉ Belisa A. Marinho
belisamarinho@gmail.com

✉ Vítor J. P. Vilar
vilar@fe.up.pt

[1] Laboratory of Separation and Reaction Engineering - Laboratory of Catalysis and Materials (LSRE-LCM), Department of Chemical Engineering, Faculty of Engineering, University of Porto, Rua do Dr. Roberto Frias, 4200-465 Porto, Portugal

[2] CAPES Foundation, Ministry of Education of Brazil, Brasília, DF 70040-020, Brazil

General aspects of arsenic and chromium

The concern about water quality and sanitation has increased during the last century. Since safe drinking water is scarce in several regions of the planet and fresh water is continuously polluted by countless contaminants, the water quality must be monitored and protected to reduce adverse health effects (Magu et al. 2016). Unlike most organic pollutants, which can be biodegradable, inorganic chemicals, including oxyanions, are continuously accumulated in the environment (Sarwar et al. 2017), posing a threat to human health due to the potential risk of entry into the food chain. The ecosystem can be contaminated with inorganic chemicals from both natural and anthropogenic activities. Industrial processes such as electroplating, metal smelting, and chemical manufacturing are examples of anthropogenic sources of inorganic chemicals in water (Chowdhury et al. 2016). In order to protect water quality, the World Health Organization (WHO) published the

first guidelines for drinking water quality in 1958 and the last update was in 2011. Additionally, other regulatory agencies have published local guidelines for drinking water quality based on the treatment performance, analytical achievability, and risks related to human health. Table 1 lists the maximum levels allowed in drinking water for some oxyanions contaminants by the European Union, US, and Brazil legislation, as well as the values suggested by WHO. The potential health effects and the common sources of each contaminant are also presented.

In water contaminated with inorganic chemicals, the options for its remediation usually require an oxidative or reductive process to achieve the less soluble or less mobile form. Arsenic and chromium are examples of oxyanions that require initially an oxidative and a reductive pre-treatment step before their removal, respectively. The most toxic and mobile arsenic species is the trivalent one, being necessary a previous oxidation to remove it from water. However, chromium in its hexavalent form is more toxic and mobile than the trivalent one, being necessary a reductive process for water remediation. Additionally, arsenic and chromium are in the top of 20 substances that pose the most significant potential threat to human health according to the Agency for Toxic Substances and Disease Registry (ATSDR 2017). Therefore, the present article briefly reviews the arsenic and chromium speciation in aqueous solutions, the analytical methods used for their detection and quantification, and the treatment processes for their removal from water. Advanced oxidation/reduction processes are highlighted.

Arsenic and chromium speciation

Arsenic is a metalloid belonging to group 15 of the periodic table. The inorganic form is mostly found in natural waters, as trivalent (As(III)) or pentavalent (As(V)) oxyanions. On the other hand, the organic arsenic can enter in the aquatic environment by both industrial pollution or biological activity (Smedley and Kinniburgh 2002). Arsenic is disposed to mobilization at a broad range of pH, including near-neutral values normally found in groundwater and in oxidizing and reducing redox potential conditions (Sarkar and Paul 2016).

The pH and redox potential (E) of the solution are the most relevant parameters as concerns arsenic speciation. The species $H_2AsO_4^-$ and $HAsO_4^{2-}$ are typically found in positive E values (oxidative conditions) and pH range from 4 to 8. At extremely lower or higher pH values, the predominant species are H_3AsO_4 and AsO_4^{3-}, respectively. However, in negative E values (reducing conditions), H_3AsO_3 predominates for acid and near-neutral pH values (pH values lower than 9.2) (Sarkar and Paul 2016). In solution, arsenate is present as H_3AsO_4, a triprotic acid, and deprotonated forms are $H_2AsO_4^-$ ($pKa_1 = 2.24$), $HAsO_4^{2-}$ ($pKa_2 = 6.96$), and AsO_4^{3-} ($pKa_3 = 11.50$) (Skoog et al. 2004), while arsenite occurs as H_3AsO_3 and its deprotonated forms are $H_2AsO_3^-$ ($pKa_1 = 9.2$) and $HAsO_3^{2-}$ ($pKa_2 = 12.7$) (Bundschuh et al. 2012; Smedley and Kinniburgh 2002). Figure 1 shows the distribution diagram of As(III) and As(V) species as a function of pH. It is worth mentioning that As(III)/As(V) ratio in groundwater is variable and depends on the aquifers oxidizing or reducing conditions. Furthermore, in contrast to other oxyanions in general, arsenic barely precipitates at near-neutral pH and its adsorption by clays or metal oxides is commonly not efficient (Sarkar and Paul 2016).

Chromium is a metal belonging to group 6 in periodic table. It can present oxidation numbers from 0 to + 6; nonetheless, only trivalent (Cr(III)) and hexavalent chromium (Cr(VI)) are stable in environmental conditions. Trivalent chromium is the most stable form in natural water conditions; however, in specific conditions, Cr(VI) can naturally occur too. The Aromas Red Sands aquifer, California, USA, is an example, where manganese oxides promote the oxidation of mineral deposits of trivalent chromium, making hexavalent chromium available in the aquifer (Gonzalez et al. 2005). While Cr(III) adsorbs on soil particles, showing low mobility and bioavailability, Cr(VI), on the other hand, is a strong oxidant, with high mobility due to its clay repulsion. In aqueous media, Cr(VI) can exist in several anionic species, mainly as chromate in deprotonated forms $HCrO_4^-$ ($pKa_1 = 0.74$) and CrO_4^{2-} ($pKa_2 = 6.49$), which are highly soluble in a wide pH range (Choppala et al. 2013). On the other hand, Cr(III) forms hydroxides with 1 to 4 hydroxyls. It starts to become insoluble at pH 6, as $Cr(OH)_3$ species is formed. However, for pH values higher than 12, it becomes soluble again. In oxygenated superficial waters, beyond pH and O_2 concentration, other parameters such as the presence of reducers, oxidants, and/or complexing agents influence the Cr(III)/Cr(VI) ratio (Kotaś and Stasicka 2000). Figure 2 shows the distribution diagram of trivalent and hexavalent chromium species as a function of pH.

Analytical techniques

Instrumental analytical methods for arsenic and chromium quantification include flame atomic absorption spectroscopy (FAAS), graphite furnace atomic absorption spectrometry (GFAAS), electrothermal atomic absorption spectrometry (ETAAS), hydride generation followed by atomic absorption spectroscopy (HG-AAS), ultraviolet-visible spectroscopy (UV-vis), inductively coupled plasma–mass spectrometry (ICP-MS), neutron activation analysis (NAA), and anodic stripping voltammetry (ASV). These techniques present limits of detection (LOD) in the order of $\mu g\ L^{-1}$ and $ng\ L^{-1}$, which are coherent with the maximum contaminant levels allowed in drinking water. Since the chemical and toxicological properties change with the oxidation states, the speciation in environmental samples is very important. For aqueous matrices, this could be simpler than for biological fluids and other complex samples (Niedzielski and Siepak 2003). However,

Table 1 Maximum level allowed in drinking water for some oxyanions by the European Union, USA and Brazil legislation, values suggested by the WHO and potential health effects and common sources of each contaminant

Contaminant		Maximum allowed contaminant level				Potential health effects	Common sources	Ref.
		EU[a]	USA[b]	Brazil[c]	WHO[d]			
Sb	($\mu g\ L^{-1}$)	5	6	5	20	Blood alterations	Fire retardants, petroleum refineries, combustion of Sb-rich coal, electronic waste	(Corrales et al. 2014), (Multani et al. 2016)
	(μM)	0.04	0.05	0.04	0.16			
As	($\mu g\ L^{-1}$)	10	10	10	10	Risk of cancer, circulatory system alterations, skin damage	Erosion of natural deposits, glass, and electronics wastes	(Rebelo and Caldas 2016)
	(μM)	0.13	0.13	0.13	0.13			
Cr	($\mu g\ L^{-1}$)	50	100	50	50	Risk of cancer, allergic dermatitis	Erosion of natural deposits, pulp mills, electroplating, textile dyeing, leather tanning, and metallurgy factories	(Khan et al. 2012), (Khlifi et al. 2013)
	(μM)	0.96	1.92	0.96	0.96			
NO_3^-	($\mu g\ L^{-1}$)	50,000	10,000	10,000	50,000	Blue baby syndrome	Erosion of natural deposits, sewage, fertilizers	(Doudrick et al. 2013), (Hérissan et al. 2017)
	(μM)	962	161	161	962			
NO_2^-	($\mu g\ L^{-1}$)	500	1000	1000	3000	Blue baby syndrome	Erosion of natural deposits, sewage, fertilizers	(Daniel et al. 2009), (Liu et al. 2017)
	(μM)	11	22	22	65			
Se	($\mu g\ L^{-1}$)	10	50	10	40	Circulatory problems, hair and fingernails loss, numbness in fingers or toes	Erosion of natural deposits, petroleum, and metal refineries, mines	(Tan et al. 2016), (Takada et al. 2008)
	(μM)	0.13	0.13	0.13	0.51			

[a] European Union Council Directive (98/83/CE, 3/11/1998)

[b] United States Environmental Protection Agency (EPA) in https://www.epa.gov/ground-water-and-drinking-water/table-regulated-drinking-water-contaminants#Inorganic

[c] Brazilian Ministry of Health (Act 2914, 12/12/2011)

[d] World Health Organization - Guidelines for drinking-water quality - 4th ed.

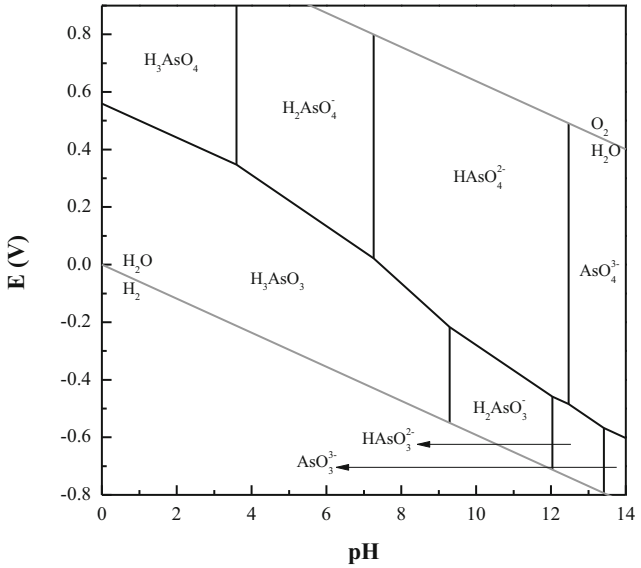

Fig. 1 Arsenic Pourbaix diagram ([As] = 0.013 mM, 25 °C, ionic strength 0.06 mM)

usually, a combination of chromatographic separation and preconcentration techniques is necessary for arsenic and chromium speciation and detection (Anawar 2012). A brief list of analytical techniques for arsenic and chromium determination is presented in Table 2.

Arsenic and chromium removal from water/wastewater

Several treatment options for water and wastewater contaminated with arsenic and chromium have been applied over the years, including chemical and electrochemical precipitation, oxidation/reduction processes, ion exchange, membrane separation, flotation, solvent extraction, evaporation, adsorption, and phytoremediation. This section contains a brief overview of treatment techniques, with special attention on advanced oxidation/reduction processes. Figure 3 summarizes some techniques for remediation of arsenic and chromium contaminated waters.

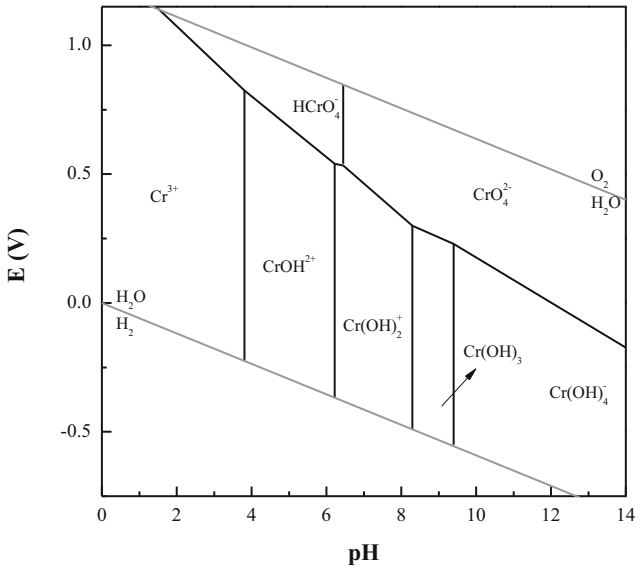

Fig. 2 Chromium Pourbaix diagram ([Cr] = 0.02 mM, 25 °C, ionic strength 0.35 mM)

Adsorption

Adsorption has been accepted as one of the most suitable treatment options due to its generally low cost, easy operation, and good efficiency. It is fundamentally a mass transfer process, where chemical or physical forces on the adsorbent surfaces drives a substance from the liquid phase to the solid phase, and the remaining adhered by bond (Song and Gallegos-Garcia 2014). In addition, an adsorption apparatus can be easily operated and there is a large availability of adsorptive materials, from the highly used activated carbon to the raw and modified biopolymeric materials (Kahu et al. 2016; Sathvika et al. 2016).

As an example, bismuth activated carbon was used for the binding of arsenite and dichromate. Arsenic removal was mainly achieved by ligand exchange, while in chromium sorption, the most important role was a metal reduction in combination with electrostatic phenomenon (Zhu et al. 2016). Activated carbon doped with iron hydroxide and manganese dioxide was used for As(III) adsorption. This material has the advantage of having a large surface area due to active carbon and oxidative property due to the presence of FeOOH and MnO_2, which allows the oxidation of trivalent to pentavalent arsenic. Under optimized conditions, the adsorption capacity of trivalent arsenic was 1 $mmol_{As}\ g_{adsorbent}^{-1}$ at pH 3 (Xiong et al. 2017). Chitosan is another material commonly used in adsorption studies. Kumar and Jiang (2016) reported the chitosan functionalization by graphene oxide to improve arsenic adsorption from aqueous solutions. They pointed out several interactions such as cationic and anionic, electrostatic, and intermolecular hydrogen bonding between the adsorbent and arsenic oxyanion species. The adsorption of As(V) in feldspars is reported to follow a pseudo-second-order kinetics and it is guided by electrostatic forces between terminal aluminol groups and arsenic in an acidic medium (Yazdani et al. 2016). However, over a macroporous polymer coated with coprecipitated iron–aluminum hydroxides, while As(III) adsorption follows a pseudo-second-order model, pentavalent species adsorption, on the other hand, follows a pseudo-first-order kinetic model. The polymer presented an adsorption capacity of 1.1 $mmol_{As}\ g_{adsorbent}^{-1}$ for As(III) and it is attributed to the formation of a bidentate mononuclear complex with iron sites. For As(V), a 0.7 $mmol_{As}\ g_{adsorbent}^{-1}$ adsorption capacity was observed as a result of generation of a bidentate binuclear complex with aluminum on the adsorbent (Suresh Kumar et al. 2016).

Table 2 Analytical techniques for arsenic and chromium determination

Species determined	Method	LOD ($\mu g\ L^{-1}$)	LOD (μM)	Ref.
Colorimetric techniques—ultraviolet-visible spectroscopy (UV-vis)				
As(V)	Molybdenum blue	1	0.013	(Tsang et al. 2007)
As, As(III), As(V)	Reduction to AsH_3 in acid solution using a hydrogen generator. The AsH_3 is absorbed in a solution of silver diethyldithiocarbamate dissolved in pyridine, forming a red complex which is detected/measured at 535 nm.	1	0.013	ISO 6595
Cr(VI)	1,5-Diphenylcarbazide	2	0.038	(Clesceri et al. 1999)
Cr, Cr(III), Cr(VI)	Oxidation of celestine blue by H_2O_2 in the presence of 2,2′-bipyridyl and cetylpyridinium chloride	0.65	0.013	(Gürkan et al. 2017)
Flame atomic absorption spectroscopy (FAAS)				
Cr(VI)	Electro-membrane extraction followed by flame atomic absorption spectrometry (IEME-FAAS)	0.003	6×10^{-5}	(Boutorabi et al. 2017)
Hydride generation followed by atomic absorption spectroscopy (HG-AAS)				
As(III)	Cloud point extraction followed by hydride generation atomic absorption spectrometry (CPE-HG-AAS)	0.008	1×10^{-4}	(Ulusoy et al. 2011)
Graphite furnace atomic absorption spectrometry (GFAAS)				
As, As(III), As(V)	Solid-phase extraction coupled with dispersive liquid–liquid microextraction based on the solidification of floating organic drop followed by graphite furnace atomic absorption spectrometry (SPE-DLLME-SFO-GFAAS)	0.003	4×10^{-5}	(Shamsipur et al. 2014)
Cr	Graphite furnace atomic absorption spectrometry (GFAAS)	0.09	0.002	(Dobrowolski et al. 2012)
Electrothermal atomic absorption spectrometry (ETAAS)				
As(III), As(V)	Solid-phase extraction with carbon nanotubes followed by electrothermal atomic absorption spectrometry (SPE-ETAAS)	0.02	3×10^{-4}	(López-García et al. 2011)
Inductively coupled plasma–mass spectrometry (ICP-MS)				
As(III), As(VI), Cr(III), Cr(VI)	High-performance liquid chromatography with inductively coupled plasma mass spectrometry (HPLC–ICP-MS)	0.18 0.22 0.11 0.17	0.002 0.003 0.002 0.003	(Jabłońska-Czapla et al. 2014)
As, Cr	Inductively coupled plasma mass spectrometry (ICP-MS)	0.01 0.01	1×10^{-4} 2×10^{-4}	(Mazurova et al. 2015)
Cr(III), Cr(VI)	High-performance liquid chromatography with inductively coupled plasma mass spectrometry (HPLC–ICP-MS)	0.1	0.002	(Catalani et al. 2015)
Inductively coupled plasma–optical emission spectroscopy (ICP-OES)				
Cr, Cr(VI)	Inductively coupled plasma optical emission spectroscopy (ICP-OES). Cr(VI) is determined after Cr(III) removal by sorption in montmorillonite	0.20	4×10^{-3}	(Frois et al. 2012)
As As(III) As(V)	Hydride generation–inductively coupled plasma optical emission spectrometry (ICP-OES). As(V) is obtained from the difference between total As and As(III)	0.38 0.07 0.37	5×10^{-3} 9×10^{-4} 5×10^{-4}	(Chooto et al. 2016)
X-ray fluorescence (XRF)				
Cr	X-ray fluorescence (XRF)	0.59	0.01	(Zheng et al. 2016)
Electroanalytical techniques				
As(III)	Differential pulse anodic stripping voltammetry (DPASV)	0.02	3×10^{-4}	(Li et al. 2012)
Cr(VI)	Photoelectrochemical sensor (PEC)	0.3	0.006	(Siavash Moakhar et al. 2017)
Others techniques				
Cr(III)	Gravity and capillary force-driven flow hemiluminescence (GCF-CL)	6.2	0.1	(Liu et al. 2016)

LOD limit of detection

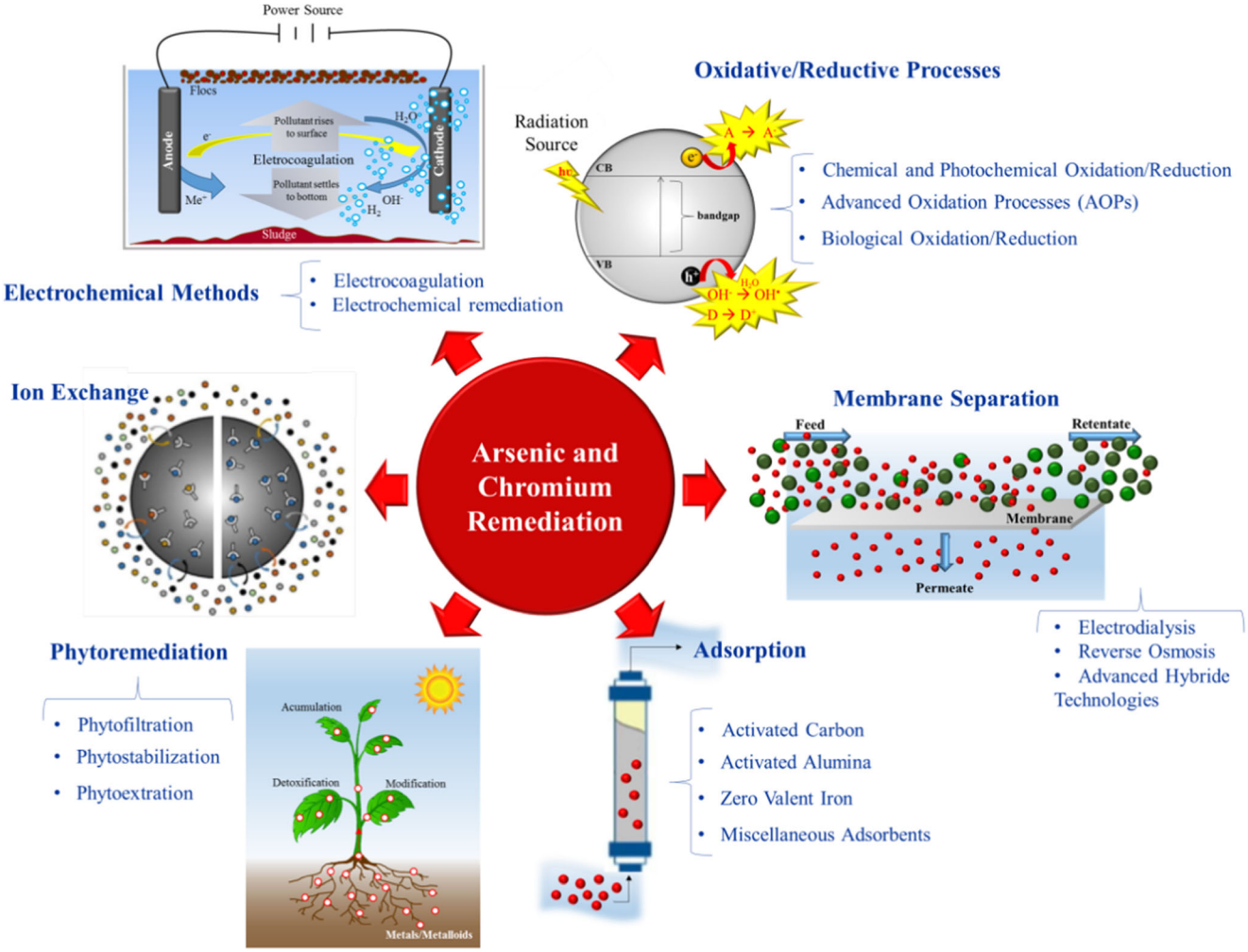

Fig. 3 Techniques for the remediation of arsenic and chromium contaminated waters. Adapted from Nidheesh and Singh (2017), Singh et al. (2010), and Mazur et al. (2017)

Zhou et al. (2016) described the application of Fe_3O_4-loaded mesoporous carbon microspheres for Cr(VI) removal. The material showed an adsorption capacity of 3 $mmol_{Cr}\ g_{adsorbent}^{-1}$ and a regeneration ability of 2.4 $mmol_{Cr}\ g_{adsorbent}^{-1}$ during five adsorption–desorption cycles. In addition, the adsorbent may be easily removed with a simple magnetic process. Moreover, the utilization of cheaper adsorbents has been focused forward conventional materials (Wu et al. 2017). Bamboo charcoal grafted by Cu^{2+}–N–aminopropylsilane complexes was used for Cr(VI) adsorption (Wu et al. 2017). The authors reported a maximum adsorption capacity of 0.3 $mmol_{Cr}\ g_{adsorbent}^{-1}$ driven by a pseudo-second-order kinetic model. Similarly, dead biomass of isolated *Aspergillus* fungal species immobilized in epichlorohydrin cross-linked cellulose showed a Cr(VI) adsorption capacity of 0.5 $mmol_{Cr}\ g_{adsorbent}^{-1}$ (Sathvika et al. 2016). In turn, low-cost adsorbent *Hibiscus cannabinus* kenaf showed a maximum Cr(VI) uptake of only 11 $\mu mol_{Cr}\ g_{adsorbent}^{-1}$ (Omidvar Borna et al. 2016). However, even though the adsorption technique has several advantages, some oxyanions have a low affinity for the adsorptive material, limiting the removal efficiency, principally when working at residual oxyanions concentrations.

Coagulation

Coagulation is defined by colloid chemistry as the aggregation of colloidal or fine particles in a medium through addition of electrolytic ions. It is commonly employed to remediation of water containing several pollutants classes (Song and Gallegos-Garcia 2014). This method, as the adsorption, presents the benefits of easy operation, cheap, and simple handling coagulants ($FeCl_3$, $FeSO_4$, $Al_2(SO_4)_3$) (Bora et al. 2016).

Since early 1970s, coagulation process for As(V) removal from water has been performed and several studies were driven to improve the process and to understand the cleaning mechanism. Currently, the use of iron or aluminum salts as

coagulants is a common process to eliminate arsenic from water (Song and Gallegos-Garcia 2014). Through the use of $NaHCO_3$, $KMnO_4$, and $FeCl_3$, 1.33 mM of arsenic was reduced to concentrations below 0.03 mM along with iron removal to concentrations below 1.8 μM (Bora et al. 2016). Using iron salts in enhanced coagulation (coagulant in excess), Cr(VI) removal can achieve almost 100% (Golbaz et al. 2014). However, coagulation processes are subject to several drawbacks including low efficiency when dealing with residual pollutants content, additional consumption of chemical reagents, and a great deal of secondary pollutants (Song et al. 2017).

Electrochemical methods

At the end of the eighteenth century, electrocoagulation was first reported to treat sewage. However, its application is still restricted due to the large initial capital investment and high energy consumption (Song et al. 2017). Usually, aluminum or iron are used as metal electrodes and according to complex precipitation kinetics, a series of hydroxides/oxyhydroxides are electrochemically formed. These species ($Fe(OH)_2$, $Fe(OH)_3$, $Al(OH)_3$, FeOOH, AlOOH) have a large surface area that can aggregate or adsorb dissolved pollutants. Parallel, hydrogen bubbles are generated by cathodic reduction and can induce flotation of the suspended particles, leading to additional pollutant removal (Nidheesh and Singh 2017).

Arsenic treatment with electrocoagulation process was studied by Vasudevan et al. (2010), using an aluminum alloy as anode and stainless steel as cathode, with a current density of 0.2 mA dm^{-2}, achieving 98.4% removal efficiency ($[As]_0 = 6.7$ μM). Beyond that, treatment of well water contaminated with arsenic in La Comarca Lagunera, México, was studied by Parga et al. (2005), using a carbon steel electrode in a pilot plant. The authors obtained 99.7% of arsenic removal attributed to magnetite formation ($[As]_0 = 6.7 \times 10^{-2}$ μM).

The recovery of an electroplating wastewater with high hexavalent chromium content by electrocoagulation was studied by Tezcan Un et al. (2017). At the best conditions (0.05 M NaCl as electrolyte, 20 mA cm^{-2}, and pH 2.4), the initial Cr(VI) concentration of 19 mM was almost completely removed over an energy consumption of 2.68 kWh m^{-3}. Additionally, the sludge obtained was used as raw material to produce reddish brown and black inorganic pigments. Hamdan and El-Naas (2014) employed Fe–Fe electrode pair to achieve 100% (considering the detection limit of the analytical method) hexavalent chromium removal ($[Cr]_0 = 3.8$ μM) in 5 min over electrocoagulation process (current density of 7.94 mA cm^{-2} and pH 8), with an estimated energy consumption of 0.6 kWh m^{-3}. Furthermore, treatment of a metal plating wastewater containing copper, chromium, and nickel (in concentrations of 0.71, 0.86, and 6.71 mM, respectively) by electrocoagulation with iron and aluminum electrodes was investigated by Akbal and Camcı (2011). At the optimum conditions, current density of 10 mA cm^{-2} and pH 3.0, a removal of 100% (considering the detection limit of the analytical method) was obtained for all three metals in 20 min, corresponding to an energy consumption of 10.07 kWh m^{-3}.

Ion exchange

Ion exchange is a physical-chemical sorption process where an ion from the solid phase is exchanged by other ion from the solution (Lee et al. 2017). It is a process with reversible interchange (Song and Gallegos-Garcia 2014).

Arsenic removal by ion exchange was tested with nanocomposite based on N-methyl-D-glucamine groups. The resin showed high arsenic removal efficiency, reaching, even in presence of interfering anions, arsenic concentrations below WHO recommendation. The equilibrium binding was well described by Langmuir isotherms and the binding capacity was approximately 0.7 $mmol_{As}\ g_{resin}^{-1}$ (Urbano et al. 2012). In other study, an amine-doped acrylic ion exchange fiber showed an ion exchange capacity of 7.5 mEq g^{-1} for As(V). In addition, the fiber exhibited a removal efficiency above 83% after nine regeneration cycles (Lee et al. 2017).

Cation and anion exchangers synthesized with long-chained cross-linking agents were reported by Kononova et al. (2015) to have an interesting selectivity and satisfactory kinetic properties, allowing 100% of chromium and manganese recovery in counter-current columns (Cr(VI) and Mn(II) initial concentrations of 0.02 and 0.09 M). Besides the complete solution purification, the valuable metal components could be returned back to the industrial process. The natural resin *Pelvetia canaliculata* was reported to allow a synergistic effect for the remediation of an electroplating wastewater containing Cr(VI) and Cr(III). The brown algae was able to reduce hexavalent to trivalent chromium at low pH values and bind by cation exchange the generated Cr(III). The protonated *P. canaliculata* showed a Cr(VI) reduction capacity of 2.3 mmol g^{-1} and a Cr(III) uptake capacity of 1.9 mmol g^{-1} (Hackbarth et al. 2016).

Membrane separation

In membrane separation process, the use of semipermeable membranes, selectively permeable to water and certain solutes, allows the separation of target particles from the solution. There are several membrane separation alternatives, including microfiltration, reverse osmosis, electrodialysis, ultrafiltration, and nanofiltration (Song and Gallegos-Garcia 2014).

Although reverse osmosis is reported as one of the most efficient alternatives to remove arsenic from contaminated waters, it is a very expensive process. As nanofiltration

requires operating pressures lower than the ones in reverse osmosis, nanofiltration process could be easily applicable. Thus, the efficiency of a nanofiltration pilot plant to remove arsenic from groundwater with natural contamination ($[As]_0 = 5.7$ μM) was evaluated. The rejection over 95% $HAsO_4^{2-}$ was achieved using a process integral evaluation at 7 bar (Saitua et al. 2011). In another study, combining coagulation by Fe(III) with microfiltration, 97% of arsenic removal was obtained at pH 7 ($[As]_0 = 2.7 \times 10^{-2}$ μM). The cost associated with this technology was evaluated as 0.066 U$/m^3 of treated water (Mólgora et al. 2013).

The fabrication of a membrane for Ni(II) and Cr(VI) nanofiltration was investigated by Hosseini et al. (2017). The membrane was fabricated with poly(acrylonitrile) as the main material and poly(ethylene glycol) and TiO_2 as additive. Under optimized conditions, nickel ($[Ni]_0 = 0.19$ mM) and chromium ($[Cr]_0 = 0.17$ mM) rejection were 87 and 83%, respectively. Moreover, using commercial composite polyamide membranes (PN40 and NF300), Gaikwad and Balomajumder (2017) obtained a Cr(VI) and fluorine rejection of 88% and 82% with PN40 and 97% and 92% with NF300 membranes, respectively (Cr and F initial concentrations of 0.10 and 0.26 mM).

However, the real application of membrane technologies has some disadvantages, such as the generation of considerable residual sludge amount, expensive energy use to ensure the system pressurization, and the need to regenerate the resin or to clean the membrane. Additionally, the associated residual by-products generated may lead to a consequently new font of secondary pollution (Ortega et al. 2017).

Phytoremediation, bioremediation, biosorption, and biofiltration

Phytoremediation comprises the use of living plants to treat a certain contaminant by bioaccumulation or to reduce its toxicity. Arsenic removal ($[As]_0 = 2.7 \times 10^{-2}$ μM) by rhizosphere of helophytes was investigated in a lab-scale wetland. An artificial domestic wastewater contaminated with arsenic was used. A better performance was observed under (i) carbon deficiency, (ii) oxidizing conditions, and (iii) elevated sulfate concentration. Arsenic mass balance indicated that 42.2% was accumulated within the roots, 17.2% remained within the gravel bed sediments, 16.2% was found in the pore water, 15.3% was in the outflow, and 9% was considered as unaccountable (Rahman et al. 2014). Nonetheless, in a horizontal subsurface flow pilot-scale constructed wetland for chromium removal, an important substrate contribution in chromium retention (61%, from an Cr initial concentration of 0.08 mM) was found, while the accumulation in plant was relatively low (0.24% in stems and leaves and 0.26% in roots) (Papaevangelou et al. 2017).

Although arsenic has an elevated human toxicity, a wide variety of microorganisms, mainly bacteria, can use it in redox reactions for growth and anaerobic respiration (Yamamura and Amachi 2014). As an example, the bacteria *Pseudomonas stutzeri TS44* contains genes for arsenite oxidation and arsenic resistance that allow the bacteria application for arsenite removal from the environment (Akhter et al. 2017). Similarly, chromium bioremediation by fungi and bacteria has been employed through biosorption, chromate reduction, and bioaccumulation. While bacteria mainly promotes Cr(VI) reduction, fungi present a good biosorption mechanism. *Bacillus methylotrophicus* was isolated from tannery sludge and used for chromate reduction. At optimized conditions, the bioremediation process showed 91.3% of Cr(VI) reduction in 48 h ($[Cr]_0 = 0.25$ mM) (Sandana Mala et al. 2015).

In an innovative biosorption process, the macroalgae *Gracilaria* and *Oedogonium* were treated with iron and transformed into Fe-biochar by slow pyrolysis. The produced Fe-biochar showed higher biosorption capacity for arsenic and molybdenum: 0.8–1.1 $mmol_{As}\ g_{sorbent}^{-1}$ and 0.7–0.8 $mmol_{Mo}\ g_{sorbent}^{-1}$, respectively (Johansson et al. 2016). In the same way, protonated *Laminaria* seaweed was appointed as effective good option of biosorbent for Cr(III) treatment in aqueous solutions, showing a maximum uptake capacity of 0.8 $mmol_{Cr}\ g_{sorbent}^{-1}$ at pH 4 (Dittert et al. 2012).

Biofilters are formed through a set of microorganisms fixed in a porous medium. The support media coated by a thin layer of iron or manganese oxides for metal/metalloid removal from water is a long-term established filtration method. However, the biological adsorptive filtration proved to be an innovative variation of this methodology. The technique consists in the use of a biofilter with native microorganisms capable to oxidize iron and manganese, which can be naturally coated on the supports. Thus, groundwater containing arsenic species can be treated by the combination of these biological/physicochemicals sorption processes: the oxidation and adsorption onto the biogenic iron and manganese oxides (Sahabi et al. 2009). In another study, As(III) removal using biological/iron/manganese combined oxidation systems leads to a decrease in arsenic concentration from 2.0 to 0.13 mM (Yang et al. 2014). The genetic diversity of microorganisms along the depth of the biofilter was investigated and the results suggested that the iron-oxidizing bacteria (*Gallionella* and *Leptothrix*), manganese-oxidizing bacteria (*Hyphomicrobium* and *Arthrobacter*), and arsenic oxidizing bacteria (*Alcaligenes* and *Pseudomonas*) were dominant in the biofilter (Yang et al. 2014).

Oxidative/reductive processes

Arsenic chemical oxidation is feasible over various oxidant agents. Zhang et al. (2017) compared As(III) oxidation

($[As]_0$ = 1.00–2.67 μM)) by potassium permanganate, sodium hypochlorite, monochloramine, and chlorine dioxide. The oxidation reactions are described by Eqs. (1), (2), (3), (4), and (5):

$$H_3AsO_3 + NaClO \rightarrow H_2AsO_4^- + Na^+ + Cl^- + H^+ \quad (1)$$

$$H_3AsO_3 + 2MnO_4^- \rightarrow 3H_2AsO_4^- + 2MnO_2 + H_2O + H^+ \quad (2)$$

$$H_3AsO_3 + 2ClO_2 + H_2O \rightarrow H_2AsO_4^- + 2ClO_2^- + 3H^+ \quad (3)$$

$$5H_3AsO_3 + 2ClO_2 + H_2O \rightarrow 5H_2AsO_4^- + 2Cl^- + 7H^+ \quad (4)$$

$$H_3AsO_3 + NH_4Cl + H_2O \rightarrow HAsO_4^{2-} + NH_4^+ + Cl^- + 2H^+ \quad (5)$$

Using the potassium permanganate and sodium hypochlorite, an As(III) oxidation of 80% was obtained after 1 and 5 min, respectively. However, using monochloramine and chlorine dioxide under similar conditions, only 70% and 50% of As(III) oxidation was achieved after 2 days (Zhang et al. 2017).

Fe(II) is widely used for hexavalent chromium reduction. CL:AIRE (2007) reported a real case of groundwater contamination with Cr(VI) (1.6 mM) where the application in situ of an acidic ferrous sulfate heptahydrate solution was capable of removing 99.95% of hexavalent chromium by a reductive precipitation mechanism. In this process, Cr(VI) was reduced to Cr(III) (Eq. (6)) and further precipitated as $Cr(OH)_3$ (Eq. (7)), at neutral pH (Hashim et al. 2011).

$$Cr^{6+} + 3Fe^{2+} \rightarrow Cr^{3+} + 3Fe^{3+} \quad (6)$$

$$Cr^{3+} + 3OH^- \rightarrow Cr(OH)_{3\,(s)} \quad (7)$$

The main disadvantage associated with this process for industrial wastewaters is related with the high amount of iron needed and the co-production of high amounts of sludge that require further treatment. Additionally, generally the ferrous ions are able to quickly reduce the hexavalent chromium at low pH values. However, rate constants of this reaction at near-neutral pH conditions have not been reported.

Among the chemical oxidation technologies, advanced oxidation processes are by definition processes where the hydroxyl radical ($^{\bullet}OH$) acts as the main oxidant agent. It is a radical with a high oxidizing potential (E^o = 2.8 V) able to react with virtually all classes of organic and inorganic compounds in relatively short times (Zhang et al. 2017). However, some AOPs techniques can also generate electrons or reductive species, which can be applied to promote reduction reactions. In the next section, these systems are discussed over their fundamental characteristics and in regard to arsenic and chromium treatment.

Advanced oxidation/reduction processes

Different reactions can lead to hydroxyl radical generation, being the most popular techniques the photolysis of hydrogen peroxide using UVC, ozonation, iron-based processes (mainly Fenton reaction), and heterogeneous photocatalysis (mainly TiO_2 as catalyst). These processes can be divided into homogeneous or heterogeneous if reactants and pollutants are in the same phase (ozonation, UVC/H_2O_2, and Fenton) or not (semiconductor/UV). They can be also differentiated in photochemical (UVC/H_2O_2, semiconductor/UV, and photo-Fenton) and non-photochemical (O_3 and Fenton), when in the presence or absence of radiation, respectively. Among the photochemical AOPs, iron-based processes and heterogeneous photocatalysis are able to initiate both oxidative and reductive processes, being applicable to promote hexavalent chromium reduction and trivalent arsenic oxidation, while UVC/H_2O_2 process is applicable only to generate $^{\bullet}OH$ radicals and, consequently, can only be used for As(III) oxidation. It should be noted that despite only the most recent references will be cited in this review work, reports on As(III) and Cr(VI) removal by the processes mentioned below have been published since many years ago.

Iron-based processes

Fenton reaction is the most used iron-based process. It is described by the reaction of ferrous ions with hydrogen peroxide (Eq. (8)). In photo-Fenton reaction, UV-vis radiation enhances $^{\bullet}OH$ radical production by forming a catalytic cycle through the photoreduction of ferric ions to ferrous ions (Eq. (9)).

$$Fe^{2+} + H_2O_2 \rightarrow Fe^{3+} + OH^- + {}^{\bullet}OH \quad (8)$$

$$Fe^{3+} + H_2O + h\nu \rightarrow Fe^{2+} + H^+ + {}^{\bullet}OH \quad (9)$$

The ferric species with higher quantum yields (ϕ - moles of product formed or reagent consumed per moles of photons absorbed) are the hydroxide complexes $Fe(OH)^{2+}$ and $Fe(RCO_2)^{2+}$, where R is an organic ligand. These species allow the photo-induced ligand-to-metal charge-transfer (LMCT) mechanism to promote Fe(II) regeneration (Rodríguez et al. 2005; Sagawe et al. 2001). Liu et al. (2007) reported the combined treatment of hexavalent chromium and bisphenol A (BPA) by Fe(III)–OH complexes in a photocatalytic system. In this study, while Cr(VI) was reduced, BPA was simultaneously oxidized, leading to a synergic effect: both Cr(VI) photocatalytic reduction and BPA degradation rates were higher in the ternary (Fe(III)/Cr(VI)/BPA) system. However, this process has some drawbacks including a strict pH control (2.8–3.5) to minimize iron oxyhydroxide precipitation and to maximize the concentration of photoactive species. Therefore, the low efficiency of these processes at neutral pH can be avoided by adding iron

complexing agents. Actually, polycarboxylates and aminopolycarboxylates are able to complex with Fe(III), which absorb light in near-UV and visible regions more efficiently than hydroxide complexes (Clarizia et al. 2017). In fact, since the beginning of the nineteenth century, the generation of reactive species by photochemical dissociation of hydroxylated Fe(III) complexes (Eq. (10)) has been reported (Nansheng et al. 1998). Depending on the organic ligand, the Fe(III) complexes exhibit different quantum yields in different wavelengths (Gernjak et al. 2006; Malato et al. 2009). Table 3 shows some Fe(III) complexes and their respective quantum yields.

$$\left[Fe^{3+}L\right] + h\nu \rightarrow \left[Fe^{3+}L\right]^{*} \rightarrow Fe^{2+} + L^{\bullet} \quad (10)$$

Summarizing, the main advantages of using ferricarboxylate complexes can be pointed as follows: (i) quantum yields higher than ferric iron–water complexes, (ii) reaction in a higher fraction of the solar spectrum (UV + visible light), and (iii) allows working at near-neutral pH values (Clarizia et al. 2017).

Besides the type of organic ligand, a strong control of iron/ligand ratio is fundamental to ensure the process efficiency. The effect of ethylenediaminetetraacetic acid (EDTA), nitrilotriacetic acid (NTA), oxalic acid, and tartaric acid ratio was investigated by De Luca et al. (2014). The authors have found that an excess of all ligands is necessary, since the photodecarboxylation is a fast process and the hydroxyl radicals formed can attack the organic ligand. This excess avoids iron precipitation and increases the catalytic activity.

Krishna et al. (2001) reported the oxidation of As(III) solution with Fenton's reagent, and the generated As(V) solution was passed through iron scrap and filtered through sand. As(III) oxidation (0.03 mM) was performed during 10 min and in the final combined process, arsenic concentration was less than 0.13 μM. Fe(II) oxidation in the presence of EDTA was reported by Wang et al. (2013). The authors observed that at acidic and neutral pH, the presence of excess EDTA inhibited As(III) oxidation, concluding that the rapid Fe(II) oxidation is not necessarily associated with a synergistic As(III) oxidation. Alternatively, Fe(III) in the presence of citrate proved to promote faster oxidation of trivalent arsenic than in citrate absence, showing that Fe(III)–$CitOH^{-}$ complex photolysis produces oxidant species more efficiently than $Fe(OH)^{2+}$ photolysis (Hug et al. 2001).

Table 3 Quantum yield for the photoreduction of Fe(III) by various carboxylic acids (Abrahamson et al. 1994)

Carboxylic acid (CA)	ϕ - CA/Fe = 5		ϕ - CA/Fe = 167
	pH = 2.7	pH = 4.0	pH = 2.9
Oxalic acid	0.65	0.30	0.32
L(+)-Tartaric acid	0.40	0.58	
Citric acid	0.28	0.45	0.17
Succinic acid			0.26
Formic acid			0.13
Acetic acid			Null

For hexavalent chromium reduction, in systems with ferricarboxylate complexes, the photoregenerated ferrous ions may reduce hexavalent chromium, and the formed reactive oxygen species are able to oxidize, simultaneously, organic molecules existent in aqueous solution. In addition, beside the reactive oxygen species, the strong reducing agent $CO_2^{\bullet-}$ could be formed by photodecarboxylation or oxidation of oxalic, citric, and tartaric acids. This radical is able to reduce Cr(VI) and enhance the reaction (Meichtry et al. 2011; Soares et al. 2015) since the pair $CO_2^{\bullet-}/CO_2$ (− 2.20 eV) (Forouzan et al. 1996) has a more negative potential than the pair Cr(VI)/Cr(III) (+ 1.33 eV) (Dittert et al. 2014). Wei et al. (2014) reported the use of iron corrosion products combined with tartaric acid in an illuminated system for hexavalent chromium reduction. This system proved to be efficient, reducing more than 90% of the initial Cr(VI) (0.2 mM) after 30 min. Moreover, Hug et al. (1997) studied hexavalent chromium photoreduction by Fe(III)–oxalate and Fe(III)–citrate complexes. The authors reported similar behavior for both acids and no precipitation of Cr(III) hydroxides, suggesting the formation of an organic Cr(III) complex with the oxidation product of oxalate or citrate. Our research group also found very important deductions concerning the reported idea whether the kinetics of Cr(VI) reduction depends on carboxylic acids structure or on α-OH number. It was found that Cr(VI) removal rate involving different organic ligands decreases in the following order: citric acid > oxalic acid > EDTA > maleic acid, proposing that there should exist a correlation between the fraction of photoactive species formed and the α-OH number of each acid, as well as with the respective quantum yield (Marinho et al. 2016). In the same paper, Fe(III)/UVA-vis/citric acid system showed to be very promising to treat a real wastewater from a galvanization process, achieving Cr(VI) photocatalytic reduction after 30 min, a better result than the one achieved with synthetic solution (Fig. 4), due to the presence of organic matter in the effluent (DOC = 5.9 mg C L^{-1}). In fact, this system contributed to the combined effect of oxyanion reduction and organic pollutant removal.

A scheme for Cr(VI) photoreduction in systems with ferricarboxylate complexes is presented in Fig. 5.

H_2O_2-UVC

Hydrogen peroxide photolysis by UVC radiation (Eq. 11) represents one of the easiest ways to produce $^{\bullet}OH$ radicals (Oppenländer 2007). This process has a powerful oxidation ability, no undesired sludge generation, and easy operation.

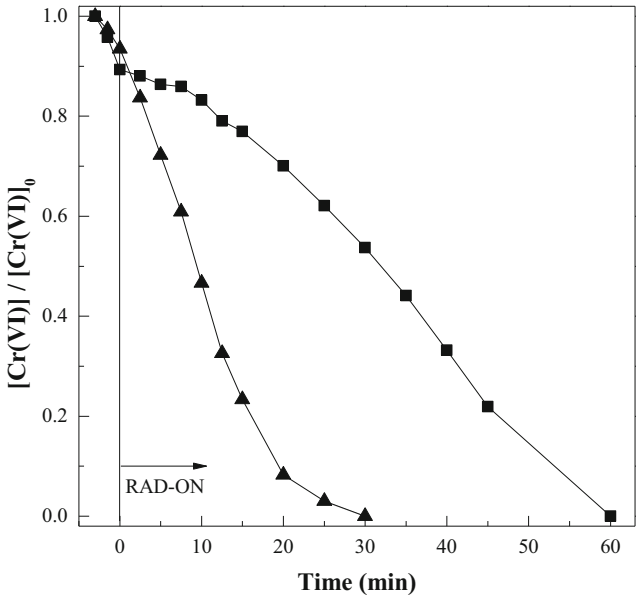

Fig. 4 Photoreduction of Cr(VI) by a Fe(III)/UVA-vis/Citric acid system with 2.4 mM of citric acid and 0.16 mM of iron at pH 5.0, 25 °C in the lab-scale photoreactor (SUNTEST at 500 W m^{-2}). (Square) synthetic Cr(VI) solution, (triangle) real wastewater

However, it involves the use of high amounts of hydrogen peroxide and stricter control of pH and temperature to prevent H_2O_2 decomposition (Eq. 12) (He et al. 2012; Rosario-Ortiz et al. 2010).

$$H_2O_2 \xrightarrow{hv} 2\ {}^{\bullet}OH \quad (11)$$

$$2H_2O_2 \rightarrow 2H_2O + O_2 \quad (12)$$

As in this process only the $^{\bullet}OH$ radical oxidant is produced, it is not applicable for Cr(VI) reduction. Concerning As(III) oxidation, the process is feasible and can even be driven "in the dark" (chemical oxidation by H_2O_2). However, Litter et al. (2010) reported that, in this case, a large excess of hydrogen peroxide is needed to reach the total oxidation. On the other hand, the As(III) oxidation by direct photolysis with UV radiation is not very efficient. Conversely, using the combined UVC/H_2O_2 process, the As(III) is improved and lower H_2O_2 doses are required when compared with dark system. In fact, Lescano et al. (2011), reported an initial H_2O_2/As(III) molar ratio in the range of 159–247 as the optimum range to promote As(III) oxidation in short reaction times. In another study, the photon flux was described to have a significant influence on the reaction rate, showing that the kinetic constant decreases linearly with the photon flux decrease (Lescano et al. 2012). In a recent work (Marinho et al. 2018b), our research group showed the successful As(III) oxidation by UVC/H_2O_2 using a micro-meso-structured photoreactor under different illumination schemes, in order to ensure a uniform irradiation of the entire reaction mixture.

Heterogeneous photocatalysis

In heterogeneous photocatalytic processes, electron (e^-_{cb}) and hole (h^+_{vb}) pairs are generated (Eq. (13)) by the absorption of photons with equal or higher energy than the photocatalyst bandgap (Wu et al. 2013). The generated holes are highly oxidizing, leading to the oxidative reaction with both organic and inorganic contaminants or to the reaction with water forming $^{\bullet}OH$ radical (Eq. (14)). In contrast, the electrons may be driven to acceptors or inorganic species with a reduction potential more positive than the one of the semiconductor conduction band (Cappelletti et al. 2008). During the last decades, due to chemical stability, low cost, and the ability to use a small percentage of ultraviolet solar radiation, TiO_2 has been the most used semiconductor in photocatalytic applications. Other semiconductors, such as ZnO, CdS, WO_3, Fe_2O_3, and SnO_2, were less investigated but can also be used. When using TiO_2 as semiconductor, in the presence of dissolved O_2 as electron acceptor, superoxide radicals ($O_2^{\bullet-}$, $HO_2^{\bullet}$) can be generated (Eqs. (15) and (16)) (Lee and Choi 2002).

$$\text{semiconductor} + hv \rightarrow e^-_{cb} + h^+_{vb} \quad (13)$$

$$OH^- + h^+_{vb} \rightarrow {}^{\bullet}OH \quad (14)$$

$$O_2 + e^-_{cb} \rightarrow O_2^{\bullet-} \quad (15)$$

$$O_2^{\bullet-} + H^+ \rightarrow HO_2^{\bullet} \quad (16)$$

Heterogeneous photocatalysis efficiency is affected by several parameters, including the initial contaminant concentration, photon flux, presence or absence of oxygen, catalyst loading, pH, and temperature. It is a consensus that the

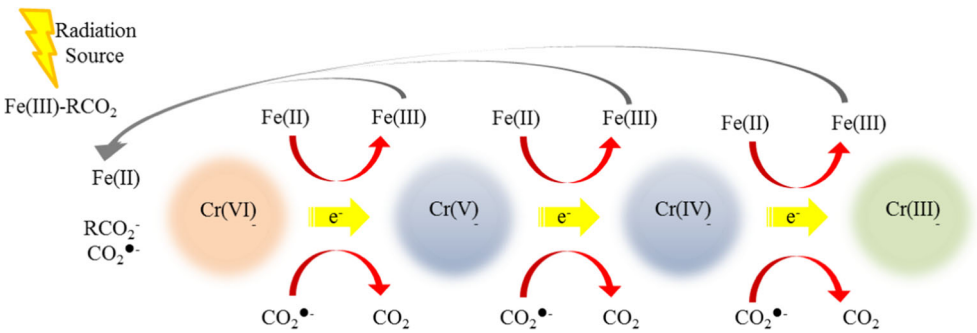

Fig. 5 Reaction scheme of an illuminated solution containing Cr(VI), carboxylic acid (as oxalic, citric or tartaric acids) and Fe(III). Adapted from Hug et al. (1997)

oxidation/reduction promoted through heterogeneous TiO_2 photocatalysis follows a first-order kinetic model. However, despite this model has been useful, it is commonly recognized that both rate constants and orders are "apparent" and also called "pseudo-first order" (Minero 1999). Above a certain photon flux, reaction rate dependency on light intensity changes from one to half-order due to the excess of photogenerated species (e^-_{cb}, h^+_{vb}, and $^{\bullet}OH$). With a further increase on the light intensity, reaction rate becomes independent. Under these conditions, the quantum yield decreases because of the high rate of e^-_{cb} /h^+_{vb} pairs recombination and the reaction rate remains constant (Malato et al. 2016). The catalyst loading influences positively the reaction rate until a certain value that depends on the photoreactor design and experimental conditions. However, above this limit, the reaction rate becomes independent of the photocatalyst load and could be negatively affected due to light attenuation caused by high catalyst quantities (Cassano and Alfano 2000). The solution pH affects significantly the TiO_2 particles charge. The pH of zero point charge (pHzpc) is defined as the pH where the particles surface is uncharged. Above this value, the catalyst is negatively charged and attracts positive molecules. At pH values below the pHzpc, the catalyst surface is positively charged attracting negative species (Fernández-Ibáñez et al. 2003). Since heterogeneous photocatalytic processes are activated by photons that reach the catalyst surface, the system does not need heating and could be conducted at room temperature. Although low temperatures favor reactants/pollutants adsorption, by-products adsorption is also enhanced, which can block the catalyst surface. In contrast, at higher temperatures, above 80 °C and near to the water boiling point, the reactants/pollutants adsorption is disfavored and may become a rate-limiting step. Additionally, the dissolved oxygen concentration in water decreases with the temperature increase. Therefore, the ideal temperature range is usually between 20 and 80 °C (Malato et al. 2016).

The reactions of a metal/metalloid with TiO_2 can be driven by three different mechanisms through successive one-electron steps: direct reduction, indirect reduction, and oxidative reaction. The direct reduction by e^-_{cb} (Eq. (17)) is viable for species with redox potential more positive than the one of e^-_{cb}. However, the reoxidation of the reduced species can cause a short circuiting (Eqs. (18) and (19)). The addition of sacrificial agents, such as organic electron donors (RH), which can be irreversibly oxidized by h^+_{vb} or $^{\bullet}OH$ (Eqs. (20) and (21)), minimizes the short circuiting and can, also, produce a synergetic effect by indirect reduction. High energetic radicals can be generated when electron donors are present (Eq. (22)). Carboxylic acids, such as formic acid and oxalic acid, can react with h^+_{vb}, acting as an electron donor and generating the strong reducing $CO_2^{\bullet-}$ radical. An oxidative reaction by h^+_{vb} (Eq. (23)) takes place when the metal/metalloid has a redox potential more negative than the h^+_{vb}. The $^{\bullet}OH$ radicals (Eq. (24)) and other species such as $O_2^{\bullet-}$, $HO_2^{\bullet}$, and H_2O_2 may also be generated and assist the oxidation (Litter 2017). Figure 6 shows a schematic diagram for the photocatalytic transformation of metal/metalloids over TiO_2 heterogeneous photocatalysis.

$$M^{n+} + e^-_{cb} \rightarrow M^{(n-1)+} \quad (17)$$

$$M^{(n-1)+} + h^+_{vb} \rightarrow M^{n+} \quad (18)$$

$$M^{(n-1)+} + {}^{\bullet}OH \rightarrow M^{n+} + OH^- \quad (19)$$

$$RH + h^+_{vb} \rightarrow R^{\bullet} + H^+ \quad (20)$$

$$RH + {}^{\bullet}OH \rightarrow R^{\bullet} + H_2O \quad (21)$$

$$R^{\bullet} + e^- + M^{n+} \rightarrow R_{ox} + M^{(n-1)+} \quad (22)$$

$$M^{n+} + h^+_{vb} \rightarrow M^{(n+1)+} \quad (23)$$

$$M^{n+} + {}^{\bullet}OH \rightarrow M^{(n+1)+} + OH^- \quad (24)$$

As(III) species can be oxidized through successive one-electron steps, by both h^+_{vb} and $^{\bullet}OH$, $O_2^{\bullet-}$ and $HO_2^{\bullet}$ radicals (Dutta et al. 2005; Guan et al. 2012; Hérissan et al. 2017; Kim et al. 2015; Lee and Choi 2002). However, the main As(III) oxidant (h^+_{vb}, $^{\bullet}OH$, $O_2^{\bullet-}$ or $HO_2^{\bullet}$) is still not clear, being the $^{\bullet}OH$ radical defended by some authors (Dutta et al. 2005; Yoon et al. 2009) and the $O_2^{\bullet-}$ /$HO_2^{\bullet}$ species by others (Choi et al. 2010; Ferguson et al. 2005; Lee and Choi 2002). Table 4 shows some studies on As(III) oxidation by heterogeneous photocatalysis.

In the last years, reduction of hexavalent to trivalent chromium using several photocatalysts has received large attention (Baig et al. 2015; Celebi et al. 2016; Chakrabarti et al. 2009; Schrank et al. 2002). Because of its high photostability, activity and reasonably low cost, TiO_2 has been widely used, both in suspension and in a supported form. Actually, Cr(VI) reduction is commonly reported to be effectively achieved by heterogeneous TiO_2 photocatalysis (Joshi and Shrivastava 2011; Testa et al. 2004). Nonetheless, in an isolated system, the formed Cr(III) can be re-oxidized to Cr(VI) by the formed holes and hydroxyl radicals. Furthermore, the electron-hole recombination may also disfavor the reaction. To suppress these effects, organic compounds are commonly added as sacrificial agents, reacting with $^{\bullet}OH$ radicals or h^+_{vb} and hindering the electron-hole recombination, contributing to an enhancement of the reduction process. In many cases, organic compounds and Cr(VI) are simultaneously present in wastewaters as a result of several industrial processes, being important to take into account their contribution. Table 5 shows some studies on hexavalent chromium reduction by heterogeneous photocatalysis.

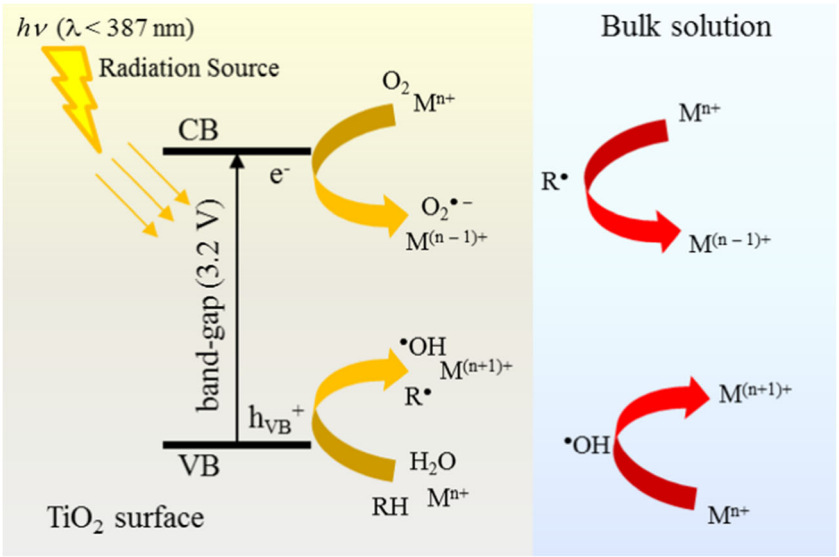

Fig. 6 Schematic diagram for the photocatalytic transformation of metal/metalloids on TiO_2. Adapted from Litter (2017)

As it is possible to see from Tables 4 and 5, the majority of publications about water treatment by heterogeneous photocatalysis are relative to the use of suspended photocatalysts. Nevertheless, it is costly and difficult to separate the catalysts from the solutions (Ananpattarachai and Kajitvichyanukul 2016). The functionalization of inert supports with photocatalysts avoids the need for a further filtration step and allowing catalyst reuse as far as its stability is maintained. In the next section, the support types and methods of catalyst immobilization are discussed.

Photocatalyst immobilization

Several methods are commonly employed to produce catalyst thin films, including chemical/physical vapor deposition, sputtering, dip-coating, sol–gel, and anodic oxidation methods (Ding et al. 2001; Monteiro et al. 2015; Pecchi et al. 2001; Sonawane et al. 2003; Vera et al. 2018). Furthermore, several types of materials including glass, paper, ceramic tiles, fiberglass, pumice stone, and stainless steel were already studied as inert supports (Ávila et al. 2002; Cardona et al. 2004; Shephard et al. 2002; Subrahmanyam et al. 2008; Vella et al. 2010). Table 6 shows some studies regarding the degradation of different contaminants using immobilized photocatalyst, as well as the coating method and support used. As an example, Han et al. (2012) used an easy and low-cost spray coating technique to successfully support TiO_2 nanoparticles over a polyester fiber filter at low temperature. Impregnation of TiO_2 in chitosan/xylan hybrid film to remove Cr(VI) through adsorption and photocatalysis was studied by Ananpattarachai and Kajitvichyanukul (2016). This innovative material presented competitive reaction rates when compared with TiO_2 powder. On the other hand, the use of polycaprolactone, a biodegradable polymer, as TiO_2 support during Cr(VI) reduction was evaluated by Akkan et al. (2015). The results a showed successful attachment of catalyst nanoparticles using simple solvent-cast processes, that lead to an efficient Cr(VI) reduction. In addition, Ferguson and Hering (2006) used glass beads coated with TiO_2 for As(III) oxidation ($[As]_0 = 2.64$ μM) in continuous flow mode, using a synthetic groundwater matrix. The authors obtained 70% of As(III) oxidation in a residence time of 10 min.

Our research group reported several studies (da Costa Filho et al. 2017; Lopes et al. 2013a; Marinho et al. 2017a; Marinho et al. 2017b; Monteiro et al. 2015; Pinho et al. 2015) on TiO_2-P25 deposition on different supports by dip and spray coating methods. It was proved that transparent cellulose acetate monolithic structures coated with TiO_2-P25 by a simple dip-coating deposition method have an effective catalytic stability during 10 consecutive Cr(VI) reduction cycles using citric acid as a hole scavenger (Marinho et al. 2017a). In other works, a reasonable good catalytic stability was observed during 3 consecutive Cr(VI) reduction cycles using TiO_2-P25 deposited both on a UV transparent cellulose acetate sheet assembled between the two slabs of a micro-meso-structured photoreactor (NETmix) (Marinho et al. 2017b) and on the front glass slab of the same reactor using a spray system. Additionally, when the catalyst is deposited on the network of channels and chambers of the NETmix reactor, despite the better performance observed, there was observed a decrease in the reaction rate in the second and third reuse cycles, which was attributed to the blockage of the catalyst surface by scavenger agents and their by-products (Marinho et al. 2018a).

Despite the several advantages of heterogeneous photocatalysis, this process also has its own drawbacks: the catalyst surface accessibility to the reactants/pollutants and photons and external mass transfer limitations, due to the higher diffusional length. The development of innovative photocatalysts with high activity and visible light response and the combination of nanosorbents with catalysts can be a good approach to improve the catalytic activity.

Table 4 Studies on the As(III) oxidation by heterogeneous photocatalysis

Pollutant	Optimal operating conditions	Efficiencies	Ref.
As(III) 1.33 μM	TiO_2–P25 = 0.05 g L^{-1} (suspended) 1000 Xe short-arc lamp UV-visible radiation Photon flux = 3×10^{-5} einstein m^{-2} s^{-1} pH range = 5–9 Total volume = 10 mL	$k = 0.1$ s^{-1} 100%[a] of As(III) oxidation in 50 s	(Bissen et al. 2001)
As(III) 200 μM	TiO_2–P25 = 0.5 g L^{-1} (suspended) 300 W Xe arc lamp UV-visible radiation ($\lambda > 300$ nm) photon flux = 3.46×10^{-3} einstein L^{-1} min^{-1} pH = 3 Total volume = 30 mL	~ 100% of As(III) oxidation in 90 min	(Choi et al. 2010)
As(III) 40 μM	TiO_2–P25 = 0.1 g L^{-1} (suspended) 125 W high-pressure mercury vapor lamp UVA (λ_{max} = 365 nm) Light intensity = 12.5 mW cm^{-2} pH = 9 Total volume = 250 mL	100%[a] of As(III) oxidation in 15 min	(Dutta et al. 2005)
As(III) 0.8 μM	TiO_2–P25 = 0.05 g L^{-1} (suspended) 8 W UVP model UVL-28 lamp UVA (λ_{max} = 365 nm) Photon flux = 1.3×10^{-7} eintein s^{-1} pH = 6.3 Total volume = 200 mL	$k = 0.005$ s^{-1} 100%[a] of As(III) Oxidation in 10 min	(Ferguson et al. 2005)
As(III) 400 μM	WO_3 = 0.5 g L^{-1} (suspended) pH = 2.5 H_2O_2 = 2 mM	~ 100% of As(III) oxidation in 90 min	(Kim et al. 2015)
As(III) 500 μM	TiO_2–P25 = 1.5 g L^{-1} (suspended) 300 W Xe arc lamp UV-visible radiation ($\lambda > 300$ nm) pH = 3 Fe(III) = 0.1 mM Total volume = 90 mL	~ 100% of As(III) oxidation in 30 min	(Lee and Choi 2002)
As(III) 75 μM	TiO_2–P25 = 0.1 g L^{-1} (suspended) 4 W Sankyodenki, F4T5BLB lamp UVA radiation ($300 < \lambda < 400$ nm) pH = 3 Total volume = 180 mL	~ 80% of As(III) oxidation in 40 min	(Yoon et al. 2009)

[a] Considering the detection limit of the analytical method

Furthermore, the reactor configuration is, also, of utmost importance regarding the system effectiveness and a competitive full-scale photocatalytic system needs to overcome mass and photons transfer limitations. This way, process intensification of heterogeneous photocatalysis through the use of innovative reactor configurations can be a good approach to enhance mass and photons transfer (Li et al. 2011). In the next section, different reactor types used in heterogeneous photocatalytic systems towards process intensification will be discussed.

Photocatalytic reactors

The industrial implementation of heterogeneous photocatalysis is limited mostly due to scale-up problems and low reaction rates. The photocatalyst reactivity in combination with photoreactor is currently in the range of 0.05–0.-1 mol $m^{-3}{}_{reactor}$ s^{-1}. However, it is suggested that this parameter should achieve 100- to 1000-fold increase before industrial implementation (Van Gerven et al. 2007). Recently, a great effort has been made towards process intensification

Table 5 Studies on the Cr(VI) reduction by heterogeneous photocatalysis

Pollutant	Optimal operating conditions	Efficiencies	Ref.
Cr(VI) 0.8 mM	TiO_2–P25 = 1 g L^{-1} (suspended) 125 W medium pressure mercury lamp UVA radiation (366 nm) Photon flux = 3.3×10^{-5} einstein s^{-1} pH = 2 Scavenger = citric acid (Cit:Cr(VI) molar equal of 1.25) Total volume = 1000 mL	$k = 0.1884$ min^{-1} ~ 99% of Cr(VI) reduction in 15 min	(Meichtry et al. 2007)
Cr(VI) 0.4 mM	TiO_2–P25 = 1 g L^{-1} (suspended) Photon flux per unit volume = 1.0×10^{-5} einstein s^{-1} L^{-1} pH = 2 Scavenger = oxalic acid (4 mM) Total volume = 20 mL	100%[a] of Cr(VI) reduction in 15 min	(Testa et al. 2004)
Cr(VI) 0.8 mM	TiO_2–P25 = 1 g L^{-1} (suspended) 8 W Philips fluorescent black light lamp UVA radiation (λ_{max} = 365 nm) Photon flux per unit volume = 95 μeinstein s^{-1} L^{-1} pH = 2 Scavenger = EDTA (2 mM) Total volume = 200 mL	$k = 0.96$ min^{-1} ~ 100% of Cr(VI) reduction in 175 s	(Meichtry et al. 2014a)
Cr(VI) 0.02 mM	TiO_2–P25 = 30 mg (supported) Solar simulator with 1700 W Xe arc lamp Intensity = 500 W m^{-2} Photon flux = 5.39×10^{-7} einstein s^{-1} pH = 3 Scavenger = tartaric acid (1.8 mM) Total volume = 1500 mL	$k = 0.047$ min^{-1} 100%[a] of Cr(VI) reduction in 60 min	(Marinho et al. 2017b)
Cr(VI) 0.8 mM	TiO_2–PC500 = 1 g L^{-1} (suspended) 8 W Philips fluorescent black light lamp UVA radiation (λ_{max} = 365 nm) Photon flux per unit volume = 95 μeinstein s^{-1} L^{-1} pH = 2 Scavenger = EDTA (2 mM) Total volume = 200 mL	$k = 1.51$ min^{-1} ~ 100% of Cr(VI) reduction in 125 s	(Meichtry et al. 2014b)
Cr(VI) 0.4 mM	TiO_2 film and a platinum anode 300 W Xe lamp Visible radiation (λ_{max} = 500 nm) Light intensity (measured by a visible radiometer) = 40 mW cm^{-2} pH = 2 Total volume = 50 mL	$k = 0.0816$ min^{-1} 99% of Cr(VI) reduction in 60 min	(Wu et al. 2013)
Cr(VI) 0.05 mM	Co-doped TiO_2 - Ti:N/I molar ratio of 1:5 = 500 mg L^{-1} (suspended) Solar simulator with 2.2 kW Xe lamp irradiation intensity = 600 W m^{-2} pH = 2; benzoic acid = 0.01 mM Total volume = 250 mL	$k = 0.171$ min^{-1} More than 90% of Cr(VI) reduction in 15 min	(Giannakas et al. 2013)
Cr(VI) 0.55 mM	TiO_2 = 2 g L^{-1} (suspended) 450 W Xe lamp UV-vis radiation (λ > 290 nm) Light intensity (measured by a radiometer in the 290–400 nm range) = 22 W m^{-2} pH = 3 Scavenger = oxalic acid (20 mM) Total volume = 150 mL	$k = 0.0346$ min^{-1} More than 90% of Cr(VI) reduction in 60 min	(Wang et al. 2004)
Cr(VI) 4 mM	CdS = 5 g L^{-1} (suspended) 250 W halogen-tungsten lamp Visible radiation Scavenger = ethanol (20%) Total volume = 20 mL	~ 100% of Cr(VI) reduction in 30 min	(Wang et al. 1992)

[a] Considering the detection limit of the analytical method

using novel reactor designs, minimizing photons and mass transfer limitations when dealing with heterogeneous photocatalytic reactions (Matsushita et al. 2008).

The first part of heterogeneous photocatalysis is the light transport to the catalyst surface. Usually, the light has to travel through the bulk solution and also through a transparent wall before reaching the catalyst surface. The amount of light that reaches the catalyst surface is only a fraction of the emitted light due to the absorption and scattering effects in reactor wall and bulk solution (Van Gerven et al. 2007). When using thin-film catalyst systems, depending on the reactor configuration, distinct irradiation mechanisms can be found: back-side

Table 6 Heterogeneous photocatalysis studies using catalyst thin films immobilized in inert supports

Photocatalyst	Support	Method	Application	Ref.
TiO_2-P25 Fe_2O_3	Kenics® static mixer	Dip or spray coating methods	Degradation of the antibiotic oxytetracycline	(Díez et al. 2018)
Nanotubular TiO_2	Pure titanium plates	Anodic oxidation at room temperature (25 °C)	Cr(VI) reduction	(Vera et al. 2018)
TiO_2-P25	Steel mesh	(i) formation of poly(vinylidene fluoride) (PVDF) binder interface by dip-coating; (ii) electrospraying of TiO_2-P25 dispersed in methanol (1 g L^{-1}); (iii) thermal fixation (160 °C and 100 MPa)	Degradation of sulfamethoxazole, reactive blue 4, methyl orange and microcystin-LR	(Ramasundaram et al. 2016)
TiO_2	Natural ceramic monoliths	Onto-the-wall extrusion, wash-coating and sol–gel methods	Chlorinated hydrocarbons oxidation	(Ávila et al. 2002)
Polyethersulfone-TiO_2 (PES/TiO_2)	Smooth glass plate	Phase inversion technique—the polymeric solution was cast on the support by a film casting knife to a thickness of 100 μm. The prepared film was immersed in a distilled water at 25 °C for 24 h, then dried at room temperature	Methyl orange degradation	(Hir et al. 2017)
TiO_2	Quartz wool	Sol–gel technique	Formic acid degradation	(Vella et al. 2010)
TiO_2-P25	Cellulose acetate sheets	Spraying (TiO_2-P25 4 wt%) and thermal fixation (50 °C)	*n*-Decane oxidation	(da Costa Filho et al. 2017)
TiO_2-P25	Pumice stone	Brushing with TiO_2 suspension (10–50 wt%) or impregnating TiO_2 suspension (10–50 wt%) with soaking, drying, and heat treatment	Disinfection (*E. coli* inactivation)	(Subrahmanyam et al. 2008)
TiO_2-loaded exterior paint	Cellulose acetate monoliths; PVC or glass tubes; glass spheres	The cellulose acetate monoliths were coated by dip-coating method; The PVC and glass tubes and glass spheres were painted in two layers with a brush	Removal of microcystin-LR	(Pinho et al. 2015)
TiO_2–ZrO_2	Glass rings	Sol–gel technique	Volatile organic compounds removal	(Hernández-Alonso et al. 2006)
TiO_2	Cellulose acetate monoliths	Sol–gel combined with dip-coating	Perchloroethylene degradation	(Lopes et al. 2013b)
Ag/TiO_2	Catalytic wall and glass rings	Dip-coating	Disinfection (*E. coli* inactivation)	(van Grieken et al. 2009)

illumination (BSI) and front-side illumination (FSI). In the BSI, the incident irradiation and the catalyst film are on opposite sides of the support structure. On the other hand, in the FSI mechanism, both incident irradiation and catalyst film are on the same side of the support structure (Chen et al. 2001). An important parameter related to the illumination is the amount of illuminated surface per unit of reaction liquid volume inside the reactor ($m^2_{ill}\ m^{-3}_{reactor}$). This value has been used quite often, although care should be taken to not neglect the shadows in the reactor and overestimate this parameter (Van Gerven et al. 2007). Table 7 lists some reactor types and their reported catalyst-coated surface per reaction liquid volume.

Once the incident light activates the catalyst, the contact between catalyst and reagents/pollutants should be maximized. One important parameter related to mass transfer is the Reynolds number, and high Reynolds numbers are associated with a decrease in mass transfer limitations (Lin and Valsaraj 2005). Several reactors design have been developed or proposed to achieve the process intensification. While slurry reactors, annular reactors, immersion reactors, optical tube reactors, and optical fiber reactors are among the most tested, some innovative reactors such as the spinning disc reactor, the monolith reactor, and the microreactor have been also tested to promote photocatalytic reactions. Figure 7 shows the schemes of some reactors applied in heterogeneous photocatalysis.

Among the various reactor types, the monolithic photoreactor is known to provide a high catalyst surface-to-volume ratio, improving the contact between the catalyst and the contaminant(s)/reactant(s), in addition to a more efficient illumination of the photocatalyst. Our team published different works on Cr(VI) reduction by heterogeneous photocatalytic processes using different reactors and system configurations. To reduce photon transfer limitations through diffusional length reduction, a tubular CPC (compound parabolic collector) photoreactor was packed with transparent cellulose acetate monolithic structures (CAM) coated with TiO_2-P25 by a dip-coating method. This reactor allows 0.15 g of TiO_2 per liter of liquid inside the photoreactor. The support geometry ensures a high surface-area-to-volume ratio, providing an illuminated catalyst surface area per unit of volume inside the reactor of 211 $m^2\ m^{-3}$. This configuration improves the contact between the photocatalyst and the contaminant(s)/reactant(s) and provides a more efficient exposure of the photocatalyst to the radiation. It was observed a photocatalyst reactivity in combination with the photoreactor of 0.09 $mmol_{Cr(VI)}\ m^{-3}_{illuminated\ volume}\ s^{-1}$, corresponding to 103 $mmol_{Cr(VI)}\ m^{-3}_{illuminated\ volume}\ kJ^{-1}$ (the values are slightly different from those published due to correction of reactor area values effectively illuminated) (Marinho et al. 2017a). On the other hand, radiant power that goes through the monolithic structure walls depends on the photocatalyst coating thickness and on the monolithic structure geometry.

Microstructured reactors are devices that allow fast mixing and short molecular diffusion distance, laminar flow, and large surface-to-volume ratio, allowing high mass transfer and reduced photon transport limitations. Therefore, it is estimated that microreactors could enhance photoreactions, in function of their higher spatial homogeneity of irradiance and better light dissemination through the entire reactor depth (Gorges et al. 2004; Padoin and Soares 2017). In this context, a novel micro-meso-structured photoreactor based on NETmix technology developed by Lopes et al. (2013b) has been successfully used by our research team (da Costa Filho et al. 2017; Marinho et al. 2017b). This NETmix reactor has a regular network of interconnected chambers and small-sized channels, allowing short molecular diffusion distances and large specific interfacial areas, improving pollutant/reactants/catalyst contact. The chambers are modeled as perfectly mixing zones and the channels as plug flow perfect segregation zones, improving the radial mixing, and, consequently, the mass and heat transfer, over a laminar flow (Fig. 8). The intensification of Cr(VI) photocatalytic reduction was tested through TiO_2-P25 deposition on UV transparent cellulose acetate (CA) sheets placed between the two slabs of the photoreactor (Marinho et al. 2017b). The micro-meso-structured reactor flat configuration and the small size of the channels and chambers provided an efficient and uniform exposure of TiO_2-P25 CA sheets to radiation, with an illuminated surface per unit of volume inside the reactor of 333 $m^2\ m^{-3}$ and 0.74 g TiO_2 per liter of liquid inside the reactor. The photocatalyst reactivity in combination with the photoreactor was significantly

Table 7 Comparison of catalyst coated surface per reaction liquid volume in different photoreactor configurations (adapted from Van Gerven et al. (2007))

Reactor type	Catalyst-coated surface per reaction liquid volume ($m^2\ m^{-3}$)	Reference
Slurry	2631	(Mukherjee and Ray 1999)
Annular or immersion	27–340	(Imoberdorf et al. 2006; Mukherjee and Ray 1999)
Optical fiber/hollow tube	46–2000	(Mukherjee and Ray 1999; Wang and Ku 2003)
Monolith	943–1333	(Lin and Valsaraj 2005; Sauer and Ollis 1994)
Spinning disc	50–130	(Raupp et al. 2001)
Microreactor	7300–14,000	(Barthe et al. 2004; Yoshihisa et al. 2006)

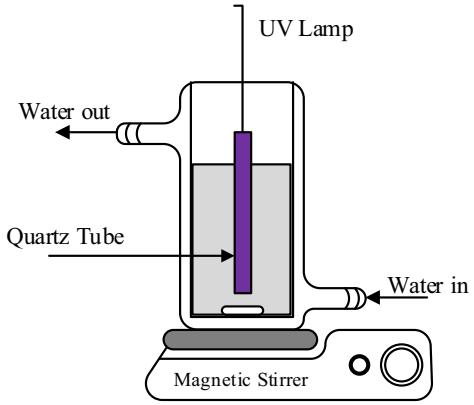
UV Lamp
Water out
Quartz Tube
Water in
Magnetic Stirrer

a)

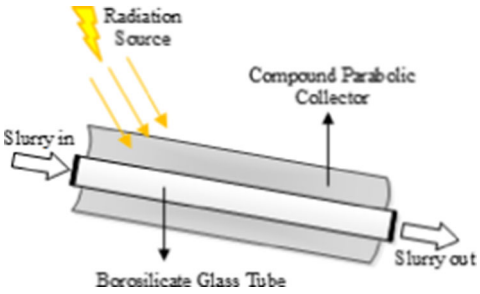
Radiation Source
Compound Parabolic Collector
Slurry in
Slurry out
Borosilicate Glass Tube

b)

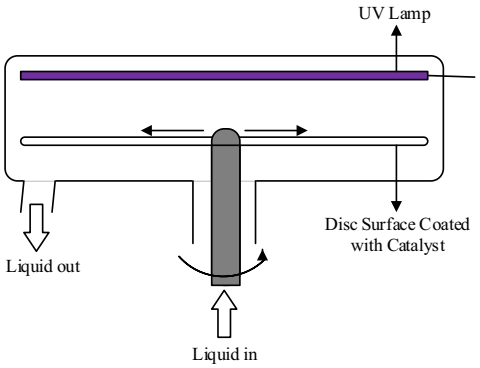
UV Lamp
Disc Surface Coated with Catalyst
Liquid out
Liquid in

c)

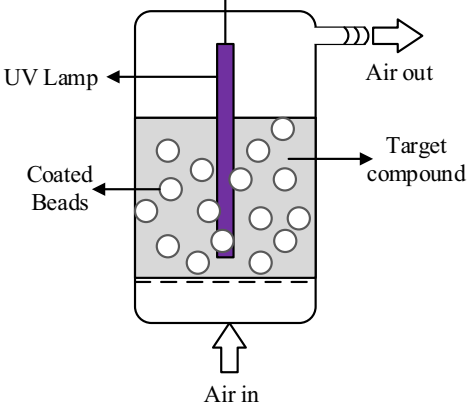
UV Lamp
Air out
Target compound
Coated Beads
Air in

d)

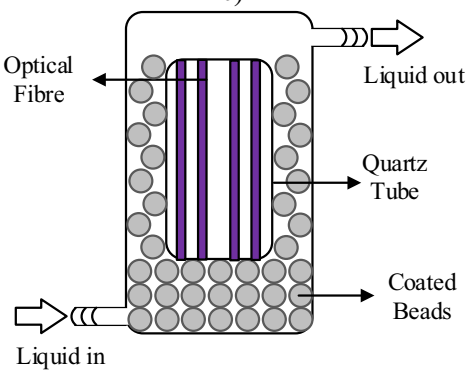
Optical Fibre
Liquid out
Quartz Tube
Coated Beads
Liquid in

e)

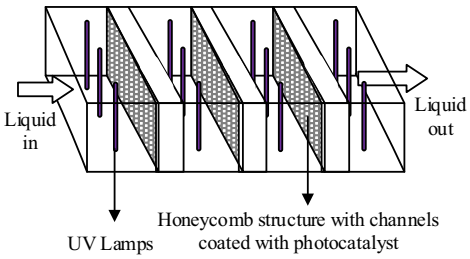
Liquid in
Liquid out
UV Lamps
Honeycomb structure with channels coated with photocatalyst

f)

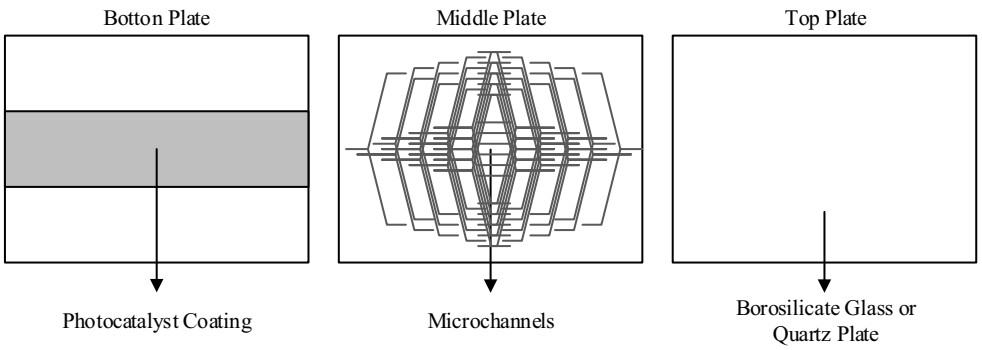
Botton Plate
Middle Plate
Top Plate
Photocatalyst Coating
Microchannels
Borosilicate Glass or Quartz Plate

g)

◀ **Fig. 7** Different reactor designs: **a** slurry immersion reactor; (**b**) slurry tubular reactor coupled with compound parabolic collector; (**c**) spinning disc reactor; (**d**) fluidized bed reactor; (**e**) side-emitting optical fiber reactor; (**f**) monolith reactor; (**g**) microreactor—Adapted from Van Gerven et al. (2007) and Boyjoo et al. (2013)

increased in relation to the monolithic tubular reactor to 1.3 $mmol_{Cr(VI)}\ m^{-3}{}_{illuminated\ volume}\ s^{-1}$ (corresponding to 2387 $mmol_{Cr(VI)}\ m^{-3}{}_{illuminated\ volume}\ kJ^{-1}$) (once more, the values are slightly different from those published due to correction of reactor area values effectively illuminated). In fact, the NETmix enhanced the shift from surface reaction to a homogeneous radical reaction, decreasing the existing mass and photons transfer limitations, probably due to the higher degree of mixing, higher amount of catalyst per unit of liquid volume, and higher spatial illumination homogeneity.

In order to evaluate BSI and FSI irradiation mechanisms, a TiO_2-P25 thin film was also uniformly deposited on the front glass slab (BSI mechanism) or on the network of channels and chambers imprinted in the back stainless steel slab (FSI mechanism) of the NETmix reactor. The results achieved with the photocatalyst immobilized at the photoreactor front glass slab (GS) are similar with the ones reported with the CA sheets as support (Marinho et al. 2017b), since the irradiation mechanism is the same for both reactor configurations (BSI mechanism). Nonetheless, a 3-fold increase on Cr(VI) reduction rate was perceived when comparing BSI and FSI irradiation mechanisms. Actually, comparing both system configurations, a 3-fold increase in the TiO_2-P25 surface area in contact with the liquid per unit of volume inside the reactor is noticed, from 333 $m^2\ m^{-3}$ when the photocatalyst is deposed on frontal glass slab to 989 $m^2\ m^{-3}$ when it is immobilized at the back stainless steel slab. Simultaneously, the photocatalyst reactivity in combination with the photoreactor was considerably improved from 2139 to 6646 $mmol_{Cr(VI)}\ m^{-3}{}_{illuminated\ volume}\ kJ^{-1}$.

In the photochemical processes, the high cost associated with energy consumption to produce UV radiation is one of the biggest problems. This drawback can be suppressed using solar radiation, with the advantages inherent in the use of a renewable, clean, and sustainable energy source. However, despite being an important source of energy, the use of solar radiation in heterogeneous photocatalysis could not be the optimal alternative for real applications due to the large area needed for the installation and operation of such reactors, the associated high cost and the dependency on the weather conditions (Braham and Harris 2009; Malato et al. 2009). As alternative, the use of a microscale illumination system based on UV-emitting diodes (UVA-LEDs) in photocatalytic reactors is known to have high illumination efficiency and to promote a larger catalyst area effectively illuminated due to their small-angle emittance (Ciambelli et al. 2009). In addition, having the advantage of having a low power input, high energy efficiency, small dimensions, and long lifetime, this irradiation source has become increasingly popular when using photochemical processes (Su et al. 2015). Thus, the intensification of heterogeneous photocatalytic processes could be achieved by combining the use of improved reactors with efficient radiation sources. As a matter of fact, a 1.2-fold increase on Cr(VI) reduction reaction rate was observed by our investigation group, when the TiO_2-P25 film immobilized in the back stainless steel slab of the NETmix reactor is irradiated by UVA-LEDs light instead of solar light. Furthermore, UVA-LED light enables the numbering up of several microreactors (compact treatment system) and significantly reduces the photon generation cost, contributing to a reasonably priced process. This system attained an almost 65-fold increase in reactivity for Cr(VI) reduction comparing with results achieved with a monolithic tubular photoreactor irradiated with simulated solar light. In Table 8 a brief comparison is made

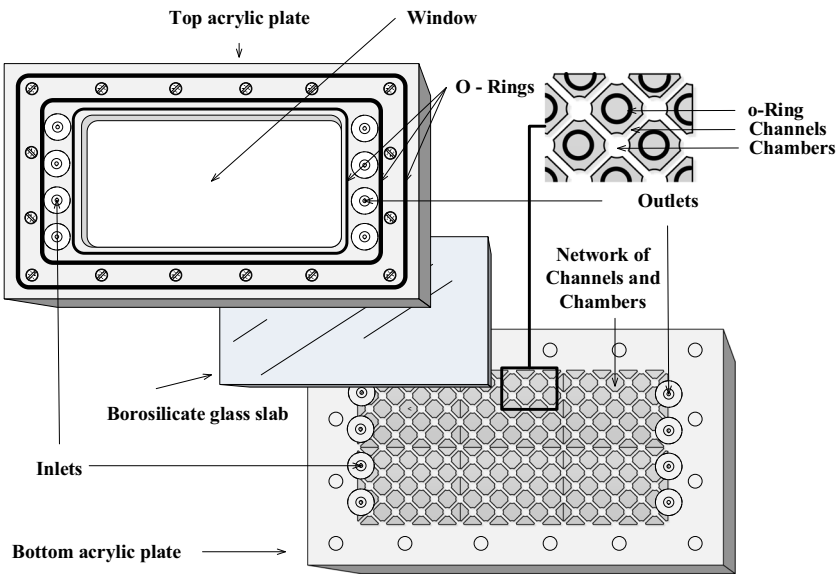

Fig. 8 Scheme of the micro-meso-structured photoreactor based on the NETmix technology. Adapted from Marinho et al. (2018a)

Table 8 Comparison of several results attained on Cr(VI) reduction (0.02 mM) by heterogeneous photocatalysis using different reactors and system configurations (Marinho et al. 2018a; Marinho et al. 2017a; Marinho et al. 2017b)

Parameters at optimized conditions	Different reactors and system configurations					
	MTP-CAM	MTP-CAM	NETmix-CA	NETmix-GS	NETmix-GS	NETmix-SSS
Radiation source	SUNTEST	SUNTEST	SUNTEST	SUNTEST	UVA-LEDs	UVA-LEDs
Illumination mechanism	BSI and FSI	BSI and FSI	BSI	BSI	BSI	FSI
Scavenger type	Citric acid	Tartaric acid	Tartaric acid	Tartaric acid	Tartaric acid	Tartaric acid
Scavenger concentration (mM)	6.9	1.8	1.8	1.8	1.8	1.8
Photocatalyst mass (mg)	40	40	30	20	20	111
Catalyst amount per illuminated volume (g L^{-1})	0.15	0.15	0.74	0.49	0.49	6.66
Illuminated area per illuminated volume (m^2 m^{-3})	211	211	333	333	333	989
k (s^{-1})	59×10^{-3}	54×10^{-3}	47×10^{-3}	45×10^{-3}	43×10^{-3}	59×10^{-3}
k (L kJ^{-1})	3.0	2.8	6.3	6.1	4.6	14.2
ξ (%)	1.94	2.00	3.96	3.84	2.84	8.82
Reactivity (mmol m^{-3} s^{-1})	0.09	0.09	1.28	1.24	1.16	3.61
Reactivity (mmol m^{-3} kJ^{-1})	102	103	2371	2321	2139	6646

between the main results obtained by our research group for the reduction of 0.02 mM of Cr(VI) by heterogeneous photocatalysis using different reactors and system configurations. Several important parameters are reported to give a clearer view of the reactor performance and to be easily compared with other systems.

Conclusions

In this review paper, arsenic and chromium speciation in solution was discussed and some analytical techniques for their determination were appointed. In addition, the current technologies to reduce and oxidize Cr(VI) and As(III), respectively, are described, especially in relation to advanced oxidation processes.

Based on the information reported, the following can be concluded:

(i). The use of advanced oxidation processes for Cr(VI) reduction and As(III) oxidation is an interesting and feasible treatment option that should be explored and enhanced.

(ii). Concerning Cr(VI) removal by heterogeneous photocatalysis in slurry systems, several papers have been published. However, there is a lack of information regarding the use of catalyst thin films and its possible reuse for Cr(VI) reduction purposes. On the other hand, although it is known that the presence of organic compounds improves the reaction and that, in most cases, they are present in wastewaters simultaneously with Cr(VI), researches regarding the treatment of real wastewaters are still scarce.

(iii). The use of advanced oxidation processes for As(III) removal is still in an early stage and much experimental work is needed for a potential application. It is necessary to clarify which are the major oxidant species responsible by As(III) oxidation.

(iv). Significant advances on intensifying heterogeneous photocatalysis are reported regarding the use of novel reactor designs, such as microreactors. Although a range of photocatalytic reactions have been carried out in novel photoreactors to date, a lot of work remains in this area, namely the theoretical modeling of oxanion removal, considering the coupling of fluid flow and mass transfer as well as photon transfer, its optimization and evaluation of scale-up strategies.

Acknowledgments V.J.P. Vilar acknowledges the FCT Investigator 2013 Programme (IF/00273/2013). B.A. Marinho acknowledges Capes for her scholarship (BEX-0983-13-6). R.O. Cristóvão thanks FCT for her Postdoc Scholarship (SFRH/BPD/101456/2014).

Funding information This work was financially supported by Project POCI-01-0145-FEDER-006984—Associate Laboratory LSRE-LCM funded by FEDER funds through COMPETE2020 - Programa Operacional Competitividade e Internacionalização (POCI)—and by national funds through FCT - Fundação para a Ciência e a Tecnologia.

References

Abrahamson HB, Rezvani AB, Brushmiller JG (1994) Photochemical and spectroscopic studies of complexes, of iron(III) with citric acid and other carboxylic acids. Inorg Chim Acta 226:117–127

Akbal F, Camcı S (2011) Copper, chromium and nickel removal from metal plating wastewater by electrocoagulation. Desalination 269: 214–222

Akhter M, Tasleem M, Mumtaz Alam M, Ali S (2017) In silico approach for bioremediation of arsenic by structure prediction and docking studies of arsenite oxidase from *Pseudomonas stutzeri* TS44. Int Biodeterior Biodegrad 122:82–91

Akkan Ş, Altın İ, Koç M, Sökmen M (2015) TiO_2 immobilized PCL for photocatalytic removal of hexavalent chromium from water. Desalin Water Treat 56:2522–2531

Ananpattarachai J, Kajitvichyanukul P (2016) Enhancement of chromium removal efficiency on adsorption and photocatalytic reduction using a bio-catalyst, titania-impregnated chitosan/xylan hybrid film. J Clean Prod 130:126–136

Anawar HM (2012) Arsenic speciation in environmental samples by hydride generation and electrothermal atomic absorption spectrometry. Talanta 88:30–42

ATSDR (2017) ATSDR's Substance Priority List

Ávila P, Sánchez B, Cardona AI, Rebollar M, Candal R (2002) Influence of the methods of TiO_2 incorporation in monolithic catalysts for the photocatalytic destruction of chlorinated hydrocarbons in gas phase. Catal Today 76:271–278

Baig U, Rao RAK, Khan AA, Sanagi MM, Gondal MA (2015) Removal of carcinogenic hexavalent chromium from aqueous solutions using newly synthesized and characterized polypyrrole–titanium(IV)phosphate nanocomposite. Chem Eng J 280:494–504

Barthe PJ, Letourneur DH, Themont JP, Woehl P (2004): Method and microfluidic reactor for photocatalysis. Google Patents

Bissen M, Vieillard-Baron M-M, Schindelin AJ, Frimmel FH (2001) TiO_2-catalyzed photooxidation of arsenite to arsenate in aqueous samples. Chemosphere 44:751–757

Bora AJ, Gogoi S, Baruah G, Dutta RK (2016) Utilization of co-existing iron in arsenic removal from groundwater by oxidation-coagulation at optimized pH. J Environ Chem Eng 4:2683–2691

Boutorabi L, Rajabi M, Bazregar M, Asghari A (2017) Selective determination of chromium(VI) ions using in-tube electro-membrane extraction followed by flame atomic absorption spectrometry. Microchem J 132:378–384

Boyjoo Y, Ang M, Pareek V (2013) Some aspects of photocatalytic reactor modeling using computational fluid dynamics. Chem Eng Sci 101:764–784

Braham RJ, Harris AT (2009) Review of major design and scale-up considerations for solar photocatalytic reactors. Ind Eng Chem Res 48: 8890–8905

Bundschuh J, Litter MI, Parvez F, Román-Ross G, Nicolli HB, Jean JS, Liu CW, López D, Armienta MA, Guilherme LRG, Cuevas AG, Cornejo L, Cumbal L, Toujaguez R (2012) One century of arsenic exposure in Latin America: a review of history and occurrence from 14 countries. Sci Total Environ 429:2–35

Cappelletti G, Bianchi CL, Ardizzone S (2008) Nano-titania assisted photoreduction of Cr(VI): the role of the different TiO_2 polymorphs. Appl Catal B Environ 78:193–201

Cardona AI, Candal R, Sánchez B, Ávila P, Rebollar M (2004) TiO_2 on magnesium silicate monolith: effects of different preparation techniques on the photocatalytic oxidation of chlorinated hydrocarbons. Energy 29:845–852

Cassano AE, Alfano OM (2000) Reaction engineering of suspended solid heterogeneous photocatalytic reactors. Catal Today 58:167–197

Catalani S, Fostinelli J, Gilberti ME, Apostoli P (2015) Application of a metal free high performance liquid chromatography with inductively coupled plasma mass spectrometry (HPLC–ICP-MS) for the determination of chromium species in drinking and tap water. Int J Mass Spectrom 387:31–37

Celebi M, Yurderi M, Bulut A, Kaya M, Zahmakiran M (2016) Palladium nanoparticles supported on amine-functionalized SiO_2 for the catalytic hexavalent chromium reduction. Appl Catal B Environ 180: 53–64

Chakrabarti S, Chaudhuri B, Bhattacharjee S, Ray AK, Dutta BK (2009) Photo-reduction of hexavalent chromium in aqueous solution in the presence of zinc oxide as semiconductor catalyst. Chem Eng J 153: 86–93

Chen D, Li F, Ray AK (2001) External and internal mass transfer effect on photocatalytic degradation. Catal Today 66:475–485

Choi W, Yeo J, Ryu J, Tachikawa T, Majima T (2010) s. Environ Sci Technol 44:9099–9104

Chooto P, Muakthong D, Innuphat C, Wararattananurak P (2016) Determination of inorganic arsenic species by hydride generation–inductively coupled plasma optical emission spectrometry. Sci Asia 42:275–282

Choppala G, Bolan N, Park JH (2013): Chapter two—chromium contamination and its risk management in complex environmental settings. In: Donald LS (ed) Advances in agronomy, vol Volume 120. Academic Press, pp 129-172

Chowdhury S, Mazumder MAJ, Al-Attas O, Husain T (2016) Heavy metals in drinking water: occurrences, implications, and future needs in developing countries. Sci Total Environ 569–570:476–488

Ciambelli P, Sannino D, Palma V, Vaiano V, Mazzei RS (2009) Improved performances of a fluidized bed photoreactor by a microscale illumination system. Int J Photoenergy 2009:7

CL:AIRE (2007) Treatment of chromium contamination and chromium ore processing residue, Technical Bulletin (TB 14). http://www.claire.co.uk

Clarizia L, Russo D, Di Somma I, Marotta R, Andreozzi R (2017) Homogeneous photo-Fenton processes at near neutral pH: a review. Appl Catal B Environ 209:358–371

Clesceri LS, Greenberg AE, Eaton AD (1999): Standard methods for the examination of water and wastewater. 20 edn. American Public Health Association, American Water Works Association, Water Environment Federation

Corrales I, Barceló J, Bech J, Poschenrieder C (2014) Antimony accumulation and toxicity tolerance mechanisms in Trifolium species. J Geochem Explor 147(Part B):167–172

da Costa Filho BM, Araujo ALP, Silva GV, Boaventura RAR, Dias MM, Lopes JCB, Vilar VJP (2017) Intensification of heterogeneous TiO_2 photocatalysis using an innovative micro-meso-structured-photoreactor for n-decane oxidation at gas phase. Chem Eng J 310:331–341

Daniel WL, Han MS, Lee J-S, Mirkin CA (2009) Colorimetric nitrite and nitrate detection with gold nanoparticle probes and kinetic end points. J Am Chem Soc 131:6362–6363

De Luca A, Dantas RF, Esplugas S (2014) Assessment of iron chelates efficiency for photo-Fenton at neutral pH. Water Res 61:232–242

Díez AM, Moreira FC, Marinho BA, Espíndola JCA, Paulista LO, Sanromán MA, Pazos M, Boaventura RAR, Vilar VJP (2018) A step forward in heterogeneous photocatalysis: process intensification by using a static mixer as catalyst support. Chem Eng J 343: 597–606

Ding Z, Hu X, Yue PL, Lu GQ, Greenfield PF (2001) Synthesis of anatase TiO_2 supported on porous solids by chemical vapor deposition. Catal Today 68:173–182

Dittert IM et al (2014) Integrated reduction/oxidation reactions and sorption processes for Cr(VI) removal from aqueous solutions using Laminaria digitata macro-algae. Chem Eng J 237:443–454

Dittert IM, Vilar VJP, da Silva EAB, de Souza SMAGU, de Souza AAU, Botelho CMS, Boaventura RAR (2012) Adding value to marine macro-algae *Laminaria digitata* through its use in the separation and recovery of trivalent chromium ions from aqueous solution. Chem Eng J 193–194:348–357

Dobrowolski R, Pawlowska-Kapusta I, Dobrzynska J (2012) Chromium determination in food by slurry sampling graphite furnace atomic absorption spectrometry using classical and permanent modifiers. Food Chem 132:597–602

Doudrick K, Yang T, Hristovski K, Westerhoff P (2013) Photocatalytic nitrate reduction in water: managing the hole scavenger and reaction by-product selectivity. Appl Catal B Environ 136–137:40–47

Dutta PK, Pehkonen SO, Sharma VK, Ray AK (2005) Photocatalytic oxidation of arsenic(III): evidence of hydroxyl radicals. Environ Sci Technol 39:1827–1834

Ferguson MA, Hering JG (2006) TiO_2-photocatalyzed As(III) oxidation in a fixed-bed, flow-through reactor. Environ Sci Technol 40:4261–4267

Ferguson MA, Hoffmann MR, Hering JG (2005) TiO_2-photocatalyzed As(III) oxidation in aqueous suspensions: reaction kinetics and effects of adsorption. Environ Sci Technol 39:1880–1886

Fernández-Ibáñez P, Blanco J, Malato S, Nieves FJD (2003) Application of the colloidal stability of TiO_2 particles for recovery and reuse in solar photocatalysis. Water Res 37:3180–3188

Forouzan F, Richards TC, Bard AJ (1996) Photoinduced reaction at TiO_2 particles Photodeposition from NiII solutions with oxalate. J Phys Chem 100:18123–18127

Frois SR, Tadeu Grassi M, de Campos MS, Abate G (2012) Determination of Cr(vi) in water samples by ICP-OES after separation of Cr(III) by montmorillonite. Anal Methods 4:4389–4394

Gaikwad MS, Balomajumder C (2017) Simultaneous rejection of chromium(VI) and fluoride [Cr(VI) and F] by nanofiltration: membranes characterizations and estimations of membrane transport parameters by CFSK model. J Environ Chem Eng 5:45–53

Gernjak W, Fuerhacker M, Fernández-Ibañez P, Blanco J, Malato S (2006) Solar photo-Fenton treatment—process parameters and process control. Appl Catal B Environ 64:121–130

Giannakas AE, Antonopoulou M, Deligiannakis Y, Konstantinou I (2013) Preparation, characterization of N–I co-doped TiO_2 and catalytic performance toward simultaneous Cr(VI) reduction and benzoic acid oxidation. Appl Catal B Environ 140:636–645

Golbaz S, Jafari AJ, Rafiee M, Kalantary RR (2014) Separate and simultaneous removal of phenol, chromium, and cyanide from aqueous solution by coagulation/precipitation: mechanisms and theory. Chem Eng J 253:251–257

Gonzalez AR, Ndung'u K, Flegal AR (2005) Natural occurrence of hexavalent chromium in the aromas Red Sands Aquifer, California. Environ Sci Technol 39:5505–5511

Gorges R, Meyer S, Kreisel G (2004) Photocatalysis in microreactors. J Photochem Photobiol A Chem 167:95–99

Guan X, Du J, Meng X, Sun Y, Sun B, Hu Q (2012) Application of titanium dioxide in arsenic removal from water: a review. J Hazard Mater 215–216:1–16

Gürkan R, Ulusoy Hİ, Akçay M (2017) Simultaneous determination of dissolved inorganic chromium species in wastewater/natural waters by surfactant sensitized catalytic kinetic spectrophotometry. Arab J Chem 10(Supplement 1):S450–S460

Hackbarth FV, Maass D, de Souza AAU, Vilar VJP, de Souza SMAGU (2016) Removal of hexavalent chromium from electroplating wastewaters using marine macroalga *Pelvetia canaliculata* as natural electron donor. Chem Eng J 290:477–489

Hamdan SS, El-Naas MH (2014) Characterization of the removal of chromium(VI) from groundwater by electrocoagulation. J Ind Eng Chem 20:2775–2781

Han Z, Chang VWC, Zhang L, Tse MS, Tan OK, Hildemann LM (2012) Preparation of TiO_2-coated polyester fiber filter by spray-coating and its photocatalytic degradation of gaseous formaldehyde. Aerosol Air Qual Res 12:1327–1335

Hashim MA, Mukhopadhyay S, Sahu JN, Sengupta B (2011) Remediation technologies for heavy metal contaminated groundwater. J Environ Manag 92:2355–2388

He X, Pelaez M, Westrick JA, O'Shea KE, Hiskia A, Triantis T, Kaloudis T, Stefan MI, de la Cruz AA, Dionysiou DD (2012) Efficient removal of microcystin-LR by UV-C/H_2O_2 in synthetic and natural water samples. Water Res 46:1501–1510

Hérissan A, Meichtry JM, Remita H, Colbeau-Justin C, Litter MI (2017) Reduction of nitrate by heterogeneous photocatalysis over pure and radiolytically modified TiO_2 samples in the presence of formic acid. Catal Today 281(Part 1):101–108

Hernández-Alonso MD, Tejedor-Tejedor I, Coronado JM, Soria J, Anderson MA (2006) Sol–gel preparation of TiO_2–ZrO_2 thin films supported on glass rings: influence of phase composition on photocatalytic activity. Thin Solid Films 502:125–131

Hir ZAM, Moradihamedani P, Abdullah AH, Mohamed MA (2017) Immobilization of TiO_2 into polyethersulfone matrix as hybrid film photocatalyst for effective degradation of methyl orange dye. Mater Sci Semicond Process 57:157–165

Hosseini SS, Nazif A, Alaei Shahmirzadi MA, Ortiz I (2017) Fabrication, tuning and optimization of poly (acrilonitryle) nanofiltration membranes for effective nickel and chromium removal from electroplating wastewater. Sep Purif Technol 187:46–59

Hug SJ, Canonica L, Wegelin M, Gechter D, von Gunten U (2001) Solar oxidation and removal of arsenic at circumneutral pH in iron containing waters. Environ Sci Technol 35:2114–2121

Hug SJ, Laubscher H-U, James BR (1997) Iron(III) catalyzed photochemical reduction of chromium(VI) by oxalate and citrate in aqueous solutions. Environ Sci Technol 31:160–170

Imoberdorf GE, Cassano AE, Alfano OM, Irazoqui HA (2006) Modeling of a multiannular photocatalytic reactor for perchloroethylene degradation in air. AICHE J 52:1814–1823

Jabłońska-Czapla M, Szopa S, Grygoyć K, Łyko A, Michalski R (2014) Development and validation of HPLC–ICP-MS method for the determination inorganic Cr, As and Sb speciation forms and its application for Pławniowice reservoir (Poland) water and bottom sediments variability study. Talanta 120:475–483

Johansson CL, Paul NA, de Nys R, Roberts DA (2016) Simultaneous biosorption of selenium, arsenic and molybdenum with modified algal-based biochars. J Environ Manag 165:117–123

Joshi KM, Shrivastava VS (2011) Photocatalytic degradation of chromium (VI) from wastewater using nanomaterials like TiO_2, ZnO, and CdS. Appl Nanosci 1:147–155

Kahu SS, Shekhawat A, Saravanan D, Jugade RM (2016) Two fold modified chitosan for enhanced adsorption of hexavalent chromium from simulated wastewater and industrial effluents. Carbohydr Polym 146:264–273

Khan FH, Ambreen K, Fatima G, Kumar S (2012) Assessment of health risks with reference to oxidative stress and DNA damage in chromium exposed population. Sci Total Environ 430:68–74

Khlifi R, Olmedo P, Gil F, Hammami B, Chakroun A, Rebai A, Hamza-Chaffai A (2013) Arsenic, cadmium, chromium and nickel in cancerous and healthy tissues from patients with head and neck cancer. Sci Total Environ 452–453:58–67

Kim D-H, Bokare AD, Koo MS, Choi W (2015) Heterogeneous catalytic oxidation of As(III) on nonferrous metal oxides in the presence of H_2O_2. Environ Sci Technol 49:3506–3513

Kononova ON, Bryuzgina GL, Apchitaeva OV, Kononov YS (2015) Ion exchange recovery of chromium (VI) and manganese (II) from aqueous solutions. Arab J Chem. In Press, Corrected Proof

Kotaś J, Stasicka Z (2000) Chromium occurrence in the environment and methods of its speciation. Environ Pollut 107:263–283

Krishna MVB, Chandrasekaran K, Karunasagar D, Arunachalam J (2001) A combined treatment approach using Fenton's reagent and zero valent iron for the removal of arsenic from drinking water. J Hazard Mater 84:229–240

Kumar ASK, Jiang S-J (2016) Chitosan-functionalized graphene oxide: a novel adsorbent an efficient adsorption of arsenic from aqueous solution. J Environ Chem Eng 4:1698–1713

Lee C-G, Alvarez PJJ, Nam A, Park S-J, Do T, Choi U-S, Lee S-H (2017) Arsenic(V) removal using an amine-doped acrylic ion exchange fiber: kinetic, equilibrium, and regeneration studies. J Hazard Mater 325:223–229

Lee H, Choi W (2002) Photocatalytic oxidation of arsenite in TiO_2 suspension: kinetics and mechanisms. Environ Sci Technol 36:3872–3878

Lescano M, Zalazar C, Cassano A, Brandi R (2012) Kinetic modeling of arsenic (III) oxidation in water employing the UV/H_2O_2 process. Chem Eng J 211–212:360–368

Lescano MR, Zalazar CS, Cassano AE, Brandi RJ (2011) Arsenic (iii) oxidation of water applying a combination of hydrogen peroxide and UVC radiation. Photochem Photobiol Sci 10:1797–1803

Li D, Li J, Jia X, Han Y, Wang E (2012) Electrochemical determination of arsenic(III) on mercaptoethylamine modified Au electrode in neutral media. Anal Chim Acta 733:23–27

Li D, Xiong K, Yang Z, Liu C, Feng X, Lu X (2011) Process intensification of heterogeneous photocatalysis with static mixer: enhanced mass transfer of reactive species. Catal Today 175:322–327

Lin H, Valsaraj KT (2005) Development of an optical fiber monolith reactor for photocatalytic wastewater treatment. J Appl Electrochem 35:699–708

Litter MI (2017) Last advances on TiO_2-photocatalytic removal of chromium, uranium and arsenic. Current Opinion in Green and Sustainable. Chemistry 6:150–158

Litter MI, Morgada ME, Bundschuh J (2010) Possible treatments for arsenic removal in Latin American waters for human consumption. Environ Pollut 158:1105–1118

Liu R, Zhang P, Li H, Zhang C (2016) Lab-on-cloth integrated with gravity/capillary flow chemiluminescence (GCF-CL): towards simple, inexpensive, portable, flow system for measuring trivalent chromium in water. Sensors Actuators B Chem 236:35–43

Liu R, Zhao J, Huang Z, Zhang L, Zou M, Shi B, Zhao S (2017) Nitrogen and phosphorus co-doped graphene quantum dots as a nano-sensor for highly sensitive and selective imaging detection of nitrite in live cell. Sensors Actuators B Chem 240:604–612

Liu Y, Deng L, Chen Y, Wu F, Deng N (2007) Simultaneous photocatalytic reduction of Cr(VI) and oxidation of bisphenol A induced by Fe(III)–OH complexes in water. J Hazard Mater 139:399–402

Lopes FVS et al (2013a) Perchloroethylene gas-phase degradation over titania-coated transparent monoliths. Appl Catal B Environ 140-141:444–456

Lopes JCB, Dos Santos Da Costa Laranjeira PEM, Dias MMGQ, Martins AAA (2013b): Network mixer and related mixing process. Google Patents

López-García I, Rivas RE, Hernández-Córdoba M (2011) Use of carbon nanotubes and electrothermal atomic absorption spectrometry for the speciation of very low amounts of arsenic and antimony in waters. Talanta 86:52–57

Magu MM, Govender PP, Ngila JC (2016) Geochemical modelling and speciation studies of metal pollutants present in selected water systems in South Africa. Physics Chem Earth, Parts A/B/C 92:44–51

Malato S, Fernández-Ibáñez P, Maldonado MI, Blanco J, Gernjak W (2009) Decontamination and disinfection of water by solar photocatalysis: recent overview and trends. Catal Today 147:1–59

Malato S, Maldonado MI, Fernández-Ibáñez P, Oller I, Polo I, Sánchez-Moreno R (2016) Decontamination and disinfection of water by solar photocatalysis: the pilot plants of the Plataforma Solar de Almeria. Mater Sci Semicond Process 42:15–23

Marinho BA, Cristóvão RO, Djellabi R, Caseiro A, Miranda SM, Loureiro JM, Boaventura RAR, Dias MM, Lopes JCB, Vilar VJP (2018a) Strategies to reduce mass and photons transfer limitations in heterogeneous photocatalytic processes: hexavalent chromium reduction studies. J Environ Manag 217:555–564

Marinho BA, Cristóvão RO, Djellabi R, Loureiro JM, Boaventura RAR, Vilar VJP (2017a) Photocatalytic reduction of Cr(VI) over TiO_2-coated cellulose acetate monolithic structures using solar light. Appl Catal B Environ 203:18–30

Marinho BA, Cristóvão RO, Loureiro JM, Boaventura RAR, Vilar VJP (2016) Solar photocatalytic reduction of Cr(VI) over Fe(III) in the presence of organic sacrificial agents. Appl Catal B Environ 192:208–219

Marinho BA et al (2017b) Intensification of heterogeneous TiO_2 photocatalysis using an innovative micro–meso-structured-reactor for Cr(VI) reduction under simulated solar light. Chem Eng J 318:76–88

Marinho BA et al. (2018b): Application of a micro-meso-structured reactor (NETmix) to promote photochemical UVC/H2O2 processes—oxidation of As(III) to As(V). Photochem Photobiol Sci

Matsushita Y, Ohba N, Kumada S, Sakeda K, Suzuki T, Ichimura T (2008) Photocatalytic reactions in microreactors. Chem Eng J 135(Supplement 1):S303–S308

Mazur LP, Pozdniakova TA, Mayer DA, de Souza SMAGU, Boaventura RAR, Vilar VJP (2017) Cation exchange prediction model for copper binding onto raw brown marine macro-algae *Ascophyllum nodosum*: batch and fixed-bed studies. Chem Eng J 316:255–276

Mazurova I, Khvaschevskaya A, Guseva N (2015) The choice of conditions for the determination of vanadium, chromium and arsenic concentration in waters by ICP-MS using collision mode. Procedia Chemistry 15:201–205

Meichtry JM, Brusa M, Mailhot G, Grela MA, Litter MI (2007) Heterogeneous photocatalysis of Cr(VI) in the presence of citric acid over TiO_2 particles: relevance of Cr(V)–citrate complexes. Appl Catal B Environ 71:101–107

Meichtry JM, Colbeau-Justin C, Custo G, Litter MI (2014a) Preservation of the photocatalytic activity of TiO_2 by EDTA in the reductive transformation of Cr(VI). Studies by Time Resolved Microwave Conductivity Catalysis. Today 224:236–243

Meichtry JM, Colbeau-Justin C, Custo G, Litter MI (2014b) TiO_2-photocatalytic transformation of Cr(VI) in the presence of EDTA: comparison of different commercial photocatalysts and studies by time resolved microwave conductivity. Appl Catal B Environ 144:189–195

Meichtry JM, Quici N, Mailhot G, Litter MI (2011) Heterogeneous photocatalytic degradation of citric acid over TiO_2: II. Mechanism of citric acid degradation. Appl Catal B Environ 102:555–562

Minero C (1999) Kinetic analysis of photoinduced reactions at the water semiconductor interface. Catal Today 54:205–216

Mólgora CC, Domínguez AM, Avila EM, Drogui P, Buelna G (2013) Removal of arsenic from drinking water: a comparative study between electrocoagulation-microfiltration and chemical coagulation-microfiltration processes. Sep Purif Technol 118:645–651

Monteiro RAR, Miranda SM, Rodrigues-Silva C, Faria JL, Silva AMT, Boaventura RAR, Vilar VJP (2015) Gas phase oxidation of n-decane and PCE by photocatalysis using an annular photoreactor packed with a monolithic catalytic bed coated with P25 and PC500. Appl Catal B Environ 165:306–315

Mukherjee PS, Ray AK (1999) Major challenges in the design of a large-scale photocatalytic reactor for water treatment. Chem Eng Technol 22:253–260

Multani RS, Feldmann T, Demopoulos GP (2016) Antimony in the metallurgical industry: a review of its chemistry and environmental stabilization options. Hydrometallurgy 164:141–153

Nansheng D, Feng W, Fan L, Mei X (1998) Ferric citrate-induced photodegradation of dyes in aqueous solutions. Chemosphere 36:3101–3112

Nidheesh PV, Singh TSA (2017) Arsenic removal by electrocoagulation process: recent trends and removal mechanism. Chemosphere 181:418–432

Niedzielski P, Siepak M (2003) Analytical methods for determining arsenic, antimony and selenium in environmental samples. Pol J Environ Stud 12:14

Omidvar Borna M, Pirsaheb M, Vosoughi Niri M, Khosravi Mashizie R, Kakavandi B, Zare MR, Asadi A (2016) Batch and column studies for the adsorption of chromium(VI) on low-cost Hibiscus

cannabinus kenaf, a green adsorbent. J Taiwan Inst Chem Eng 68: 80–89

Oppenländer T (2007): AOPs and AOTs. In: Photochemical purification of water and air. Wiley-VCH Verlag GmbH & Co. KGaA, pp 5–17

Ortega A, Oliva I, Contreras KE, González I, Cruz-Díaz MR, Rivero EP (2017) Arsenic removal from water by hybrid electro-regenerated anion exchange resin/electrodialysis process. Sep Purif Technol 184: 319–326

Padoin N, Soares C (2017) An explicit correlation for optimal TiO_2 film thickness in immobilized photocatalytic reaction systems. Chem Eng J 310(Part 2):381–388

Papaevangelou VA, Gikas GD, Tsihrintzis VA (2017) Chromium removal from wastewater using HSF and VF pilot-scale constructed wetlands: overall performance, and fate and distribution of this element within the wetland environment. Chemosphere 168:716–730

Parga JR et al (2005) Arsenic removal via electrocoagulation from heavy metal contaminated groundwater in La Comarca Lagunera México. J Hazard Mater 124:247–254

Pecchi G, Reyes P, Sanhueza P, Villaseñor J (2001) Photocatalytic degradation of pentachlorophenol on TiO_2 sol–gel catalysts. Chemosphere 43:141–146

Pinho LX et al (2015) Oxidation of microcystin-LR and cylindrospermopsin by heterogeneous photocatalysis using a tubular photoreactor packed with different TiO_2 coated supports. Chem Eng J 266:100–111

Rahman KZ, Wiessner A, Kuschk P, van Afferden M, Mattusch J, Müller RA (2014) Removal and fate of arsenic in the rhizosphere of *Juncus effusus* treating artificial wastewater in laboratory-scale constructed wetlands. Ecol Eng 69:93–105

Ramasundaram S, Seid MG, Choe JW, Kim EJ, Chung YC, Cho K, Lee C, Hong SW (2016) Highly reusable TiO_2 nanoparticle photocatalyst by direct immobilization on steel mesh via PVDF coating, electrospraying, and thermal fixation. Chem Eng J 306: 344–351

Raupp GB, Alexiadis A, Hossain MM, Changrani R (2001) First-principles modeling, scaling laws and design of structured photocatalytic oxidation reactors for air purification. Catal Today 69:41–49

Rebelo FM, Caldas ED (2016) Arsenic, lead, mercury and cadmium: toxicity, levels in breast milk and the risks for breastfed infants. Environ Res 151:671–688

Rodríguez M, Malato S, Pulgarin C, Contreras S, Curcó D, Giménez J, Esplugas S (2005) Optimizing the solar photo-Fenton process in the treatment of contaminated water. Determination of intrinsic kinetic constants for scale-up. Sol Energy 79:360–368

Rosario-Ortiz FL, Wert EC, Snyder SA (2010) Evaluation of UV/H_2O_2 treatment for the oxidation of pharmaceuticals in wastewater. Water Res 44:1440–1448

Sagawe G, Lehnard A, Lübber M, Bahnemann D (2001) The insulated solar Fenton hybrid process: fundamental investigations. Helvetica Chimica Acta 84:3742–3759

Sahabi DM, Takeda M, Suzuki I, Koizumi J-I (2009) Adsorption and abiotic oxidation of arsenic by aged biofilter media: equilibrium and kinetics. J Hazard Mater 168:1310–1318

Saitua H, Gil R, Padilla AP (2011) Experimental investigation on arsenic removal with a nanofiltration pilot plant from naturally contaminated groundwater. Desalination 274:1–6

Sandana Mala JG, Sujatha D, Rose C (2015) Inducible chromate reductase exhibiting extracellular activity in Bacillus methylotrophicus for chromium bioremediation. Microbiol Res 170:235–241

Sarkar A, Paul B (2016) The global menace of arsenic and its conventional remediation—a critical review. Chemosphere 158:37–49

Sarwar N et al (2017) Phytoremediation strategies for soils contaminated with heavy metals: modifications and future perspectives. Chemosphere 171:710–721

Sathvika T, Manasi, Rajesh V, Rajesh N (2016) Adsorption of chromium supported with various column modelling studies through the synergistic influence of Aspergillus and cellulose. J Environ Chem Eng 4:3193–3204

Sauer ML, Ollis DF (1994) Acetone oxidation in a photocatalytic monolith reactor. J Catal 149:81–91

Schrank SG, José HJ, Moreira RFPM (2002) Simultaneous photocatalytic Cr(VI) reduction and dye oxidation in a TiO_2 slurry reactor. J Photochem Photobiol A Chem 147:71–76

Shamsipur M, Fattahi N, Assadi Y, Sadeghi M, Sharafi K (2014) Speciation of As(III) and As(V) in water samples by graphite furnace atomic absorption spectrometry after solid phase extraction combined with dispersive liquid–liquid microextraction based on the solidification of floating organic drop. Talanta 130:26–32

Shephard GS, Stockenström S, de Villiers D, Engelbrecht WJ, Wessels GFS (2002) Degradation of microcystin toxins in a falling film photocatalytic reactor with immobilized titanium dioxide catalyst. Water Res 36:140–146

Siavash Moakhar R, Goh GKL, Dolati A, Ghorbani M (2017) Sunlight-driven photoelectrochemical sensor for direct determination of hexavalent chromium based on Au decorated rutile TiO_2 nanorods. Appl Catal B Environ 201:411–418

Singh M, Singh AK, Swati SN, Singh S, Chowdhary AK (2010) Arsenic mobility in fluvial environment of the Ganga Plain, northern India. Environ Earth Sci 59:1703–1715

Skoog DA, West DM, Holler FJ, Crouch SR (2004) Fundamentals of analytical chemitry. Brooks/Cole, Belmont

Smedley PL, Kinniburgh DG (2002) A review of the source, behaviour and distribution of arsenic in natural waters. Appl Geochem 17:517–568

Soares PA, Batalha M, Souza SMAGU, Boaventura RAR, Vilar VJP (2015) Enhancement of a solar photo-Fenton reaction with ferric-organic ligands for the treatment of acrylic-textile dyeing wastewater. J Environ Manag 152:120–131

Sonawane RS, Hegde SG, Dongare MK (2003) Preparation of titanium(IV) oxide thin film photocatalyst by sol–gel dip coating. Mater Chem Phys 77:744–750

Song P, Yang Z, Zeng G, Yang X, Xu H, Wang L, Xu R, Xiong W, Ahmad K (2017) Electrocoagulation treatment of arsenic in wastewaters: a comprehensive review. Chem Eng J 317:707–725

Song S, Gallegos-Garcia M (2014): Chapter 11—arsenic removal from water by the coagulation process A2 - Fanun, Monzer. In: The role of colloidal systems in environmental protection. Elsevier, Amsterdam, pp 261–277

Su Y, Talla A, Hessel V, Noël T (2015) Controlled photocatalytic aerobic oxidation of thiols to disulfides in an energy-efficient photomicroreactor. Chem Eng Technol 38:1733–1742

Subrahmanyam M, Boule P, Durga Kumari V, Naveen Kumar D, Sancelme M, Rachel A (2008) Pumice stone supported titanium dioxide for removal of pathogen in drinking water and recalcitrant in wastewater. Sol Energy 82:1099–1106

Suresh Kumar P, Flores RQ, Sjöstedt C, Önnby L (2016) Arsenic adsorption by iron–aluminium hydroxide coated onto macroporous supports: insights from X-ray absorption spectroscopy and comparison with granular ferric hydroxides. J Hazard Mater 302:166–174

Takada T, Hirata M, Kokubu S, Toorisaka E, Ozaki M, Hano T (2008) Kinetic study on biological reduction of selenium compounds. Process Biochem 43:1304–1307

Tan LC, Nancharaiah YV, van Hullebusch ED, Lens PNL (2016) Selenium: environmental significance, pollution, and biological treatment technologies. Biotechnol Adv 34:886–907

Testa JJ, Grela MA, Litter MI (2004) Heterogeneous photocatalytic reduction of chromium(VI) over TiO_2 particles in the presence of oxalate: involvement of Cr(V) species. Environ Sci Technol 38: 1589–1594

Tezcan Un U, Onpeker SE, Ozel E (2017) The treatment of chromium containing wastewater using electrocoagulation and the production

of ceramic pigments from the resulting sludge. J Environ Manag 200:196–203

Tsang S, Phu F, Baum MM, Poskrebyshev GA (2007) Determination of phosphate/arsenate by a modified molybdenum blue method and reduction of arsenate by $S_2O_4^{2-}$. Talanta 71:1560–1568

Ulusoy Hİ, Akçay M, Ulusoy S, Gürkan R (2011) Determination of ultra trace arsenic species in water samples by hydride generation atomic absorption spectrometry after cloud point extraction. Anal Chim Acta 703:137–144

Urbano BF, Rivas BL, Martinez F, Alexandratos SD (2012) Water-insoluble polymer–clay nanocomposite ion exchange resin based on N-methyl-d-glucamine ligand groups for arsenic removal. React Funct Polym 72:642–649

Van Gerven T, Mul G, Moulijn J, Stankiewicz A (2007) A review of intensification of photocatalytic processes. Chem Eng Process Process Intensif 46:781–789

van Grieken R, Marugán J, Sordo C, Martínez P, Pablos C (2009) Photocatalytic inactivation of bacteria in water using suspended and immobilized silver-TiO_2. Appl Catal B Environ 93:112–118

Vasudevan S, Lakshmi J, Sozhan G (2010) Studies on the removal of arsenate by electrochemical coagulation using aluminum alloy anode CLEAN – Soil, Air. Water 38:506–515

Vella G, Imoberdorf GE, Sclafani A, Cassano AE, Alfano OM, Rizzuti L (2010) Modeling of a TiO_2-coated quartz wool packed bed photocatalytic reactor. Appl Catal B Environ 96:399–407

Vera ML, Traid HD, Henrikson ER, Ares AE, Litter MI (2018) Heterogeneous photocatalytic Cr(VI) reduction with short and long nanotubular TiO2 coatings prepared by anodic oxidation. Mater Res Bull 97:150–157

Wang S, Wang Z, Zhuang Q (1992) Photocatalytic reduction of the environmental pollutant CrVI over a cadmium sulphide powder under visible light illumination. Appl Catal B Environ 1:257–270

Wang W, Ku Y (2003) Photocatalytic degradation of gaseous benzene in air streams by using an optical fiber photoreactor. J Photochem Photobiol A Chem 159:47–59

Wang X, Pehkonen SO, Ray AK (2004) Removal of aqueous Cr(VI) by a combination of photocatalytic reduction and coprecipitation. Ind Eng Chem Res 43:1665–1672

Wang Z, Bush RT, Liu J (2013) Arsenic(III) and iron(II) co-oxidation by oxygen and hydrogen peroxide: divergent reactions in the presence of organic ligands. Chemosphere 93:1936–1941

Wei S, Li J, Liu L, Shi J, Shao Z (2014) Photocatalytic effect of iron corrosion products on reduction of hexavalent chromium by organic acids. J Taiwan Inst Chem Eng 45:2659–2663

Wu Q, Zhao J, Qin G, Wang C, Tong X, Xue S (2013) Photocatalytic reduction of Cr(VI) with TiO_2 film under visible light. Appl Catal B Environ 142:142–148

Wu Y, Ming Z, Yang S, Fan Y, Fang P, Sha H, Cha L (2017) Adsorption of hexavalent chromium onto bamboo charcoal grafted by Cu^{2+}-N-aminopropylsilane complexes: optimization, kinetic, and isotherm studies. J Ind Eng Chem 46:222–233

Xiong Y, Tong Q, Shan W, Xing Z, Wang Y, Wen S, Lou Z (2017) Arsenic transformation and adsorption by iron hydroxide/manganese dioxide doped straw activated carbon. Appl Surf Sci 416:618–627

Yamamura S, Amachi S (2014) Microbiology of inorganic arsenic: from metabolism to bioremediation. J Biosci Bioeng 118:1–9

Yang L, Li X, Chu Z, Ren Y, Zhang J (2014) Distribution and genetic diversity of the microorganisms in the biofilter for the simultaneous removal of arsenic, iron and manganese from simulated groundwater. Bioresour Technol 156:384–388

Yazdani M, Tuutijärvi T, Bhatnagar A, Vahala R (2016) Adsorptive removal of arsenic(V) from aqueous phase by feldspars: kinetics, mechanism, and thermodynamic aspects of adsorption. J Mol Liq 214:149–156

Yoon S-H, Oh S-E, Yang JE, Lee JH, Lee M, Yu S, Pak D (2009) TiO_2 photocatalytic oxidation mechanism of As(III). Environ Sci Technol 43:864–869

Yoshihisa M, Shinji K, Kazuhito W, Kosaku S, Teijiro I (2006) Photocatalytic reduction in microreactors. Chem Lett 35:410–411

Zhang P, Yao W, Yuan S (2017) Citrate-enhanced release of arsenic during pyrite oxidation at circumneutral conditions. Water Res 109: 245–252

Zheng F, Lin X, Yu H, Li S, Huang X (2016) Visible-light photoreduction, adsorption, matrix conversion and membrane separation for ultrasensitive chromium determination in natural water by X-ray fluorescence. Sensors Actuators B Chem 226:500–505

Zhou J, Wang Y, Wang J, Qiao W, Long D, Ling L (2016) Effective removal of hexavalent chromium from aqueous solutions by adsorption on mesoporous carbon microspheres. J Colloid Interface Sci 462:200–207

Zhu N, Yan T, Qiao J, Cao H (2016) Adsorption of arsenic, phosphorus and chromium by bismuth impregnated biochar: adsorption mechanism and depleted adsorbent utilization. Chemosphere 164:32–40